MSRJ

UNIVERSITY OF TEXAS AT ARLINGTON

MCNAIR SCHOLARS RESEARCH JOURNAL 2018

VOL. 22

Preparing UTA students for careers in research and teaching since 1990

UNIVERSITY OF TEXAS ARLINGTON

University of Texas at Arlington McNair Scholars Research Journal

Volume 22 • 2018

Preparing UTA Students for Careers in Research and Teaching since 1990

Publication Design and Formatting by Brittany Griffiths
Cover Design by Candy McCormic

Published and made openly accessible by:
University of Texas at Arlington Libraries
702 Planetarium Pl,
Arlington, TX 76019

Print ISSN 2642-2484
Digital ISSN 2642-2492

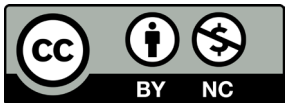

Mavs Open Press

MSRJ

UNIVERSITY OF TEXAS AT ARLINGTON
MCNAIR SCHOLARS RESEARCH JOURNAL 2018

Introduction

Papers

Abstracts

MESSAGE

FROM THE VICE PRESIDENT OF RESEARCH

Duane Dimos, Ph.D.

As university education is essential to providing a strong foundation for the future of society, university research is vital to the discovery, invention, and innovation driving our world. UT Arlington's commitment to being 'The Model 21st Century Urban Research University' is reflected in our strategic plan Bold Solutions | Global Impact. As a nationally-ranked research-1 university, our vision reflects the way in which education and research come together to meet the needs of our students and our community. The vision also highlights our strategic research areas and how they support the overarching goal of 'Global Impact Through Enabling a Sustainable Megacity', which is important to our region as the Dallas-Ft. Worth-Arlington metroplex heads quickly toward becoming a megacity.

Obtaining a PhD degree is a tremendous accomplishment, which can open a wide range of career opportunities. However, getting a PhD takes a lot of hard work and study, long hours of research, and tremendous dedication and persistence. Engaging in research as an undergraduate can give you the preparation needed to be a successful PhD student, if research is a passion for you.

The McNair Scholars Program plays an important role at UTA in providing the experiential learning to prepare promising students from low-income/first-generation or under-represented backgrounds for a successful transition to a PhD program. The program helps students realize their dreams and ambitions by providing the academic support, mentoring and research opportunities necessary to become more competitive in applying for a PhD program and to be well prepared to start their graduate work.

The efforts that prepare students to earn a doctoral degree, which the McNair Scholars Program helps accomplish, establish a foundation for a lifetime of discoveries and contributions that will shape our future. These students will be the innovators and entrepreneurs who develop the technologies that transform the results of those discoveries into improvements in health, education, and economic growth.

The University of Texas at Arlington is proud to be a supporter of the McNair Scholars Program, which has provided opportunities to so many undergraduates over the last 30 years to help them reach their full academic and professional potential. Those of us who have been privileged to work with McNair Scholars and to witness the transformation

from students to scholars are impressed with their sophistication and, as mentors, take great pride in their accomplishments. A special thanks to the faculty who have mentored them. At UTA, we are also proud to have several previous McNair Scholars from other institutions as members of our faculty.

Congratulations Scholars on your acceptance into the program. You have completed impressive work. It is work that portends an exciting future for you and for the promise your future contributions will make.

NOTES

FROM THE DIRECTOR

Joan Reinhardt, Ph.D.

I congratulate UTA McNair Scholars on their excellent research during summer 2018. Their success was due to their intelligence, creativity and tenacity and, of course, the guidance and encouragement of their faculty mentors. The majority of current Scholars will graduate this academic year and, after a short break, commence their advanced studies, here or elsewhere in the United States. Obviously, their final semesters on campus will be extremely busy, as they take the GRE, attend conferences, submit their graduate school applications, and complete their degree requirements. I am pleased to see our Scholars advance towards their goals and begin the next phase of their education. New Scholars will join the McNair program in early spring semester to fill positions vacated by those who graduate this year. During its almost thirty years at UTA, many Scholars have passed through this program to achieve great things. I anticipate that current McNair Scholars will follow their example.

The McNair Scholars program is a federal initiative to open the door to academic and professional opportunities for undergraduates from first-generation/low-income and/or underrepresented ethnicities (at the graduate level of study). In the 2018 edition of The University of Texas at Arlington McNair Scholars Research Journal, fifteen Scholars present to you the results of their work. I hope that you will find it as fascinating and informative as I have. Once again, UTA undergraduates reveal how much they can achieve when offered the opportunity and encouragement to do so. The value of such experiential learning is truly significant for the undergraduates who choose to engage in it.

In conclusion, I would like to thank President Vistasp Karbhari, Provost Teik Lim, Vice President for Research Duane Dimos, and Dean of the Library Rebecca Bichel, in addition to the McNair Selection Committee and faculty mentors, for their commitment to this program.

ABOUT

THE MCNAIR SCHOLARS PROGRAM

Dr. Ronald E. McNair
Scientist & Astronaut, 1950-1986

The McNair Scholars Program (officially known as the Ronald E. McNair Post-Baccalaureate Achievement Program) came to the campus of The University of Texas at Arlington in 1990. Created by the U.S. Congress in 1988, it is named after Dr. Ronald E. McNair, who perished with his fellow astronauts on the space shuttle Challenger two years earlier. The McNair program endeavors to assist talented undergraduates – either first generation and low-income or underrepresented students – to prepare for graduate study leading to the Ph.D. and the professoriate.

Since its beginning at UT Arlington, the McNair program has encouraged and assisted over 300 students in various majors. Currently, it works with 34 students each academic year, providing seminars and classes on topics related to graduate school and the GRE, a May institute to heighten scholars' understanding of the culture of research, and a summer research internship. The program also provides guidance with the graduate school application process and travel funds to participate in conferences and visit prospective graduate programs. UT Arlington McNair graduates have subsequently earned masters and doctorates not only from their alma mater, but also from an impressive array of universities including Harvard, Indiana, Rice, and Southern Methodist, among others.

The McNair Scholars Program enjoys strong support from the UT Arlington administration and greatly benefits from the expertise and enthusiasm of both faculty and staff. Faculty members who serve on the McNair Selection Committee and those who act as mentors to McNair interns deserve special recognition. Members of the 2017-2018 Selection Committee include the following UTA faculty and staff: Dr. Karishma Chatterjee (Communication), Dr. Laureano Hoyos (Civil Engineering), Dr. Amber Schroeder (Pyschology), Dr. Raymond (Joe) Jackson (Office of Graduate Studies), and Dr. Debra Woody (Social Work).

McNair Staff Members

Joan Reinhardt, Ph.D.
Director

Cheri Counts
Administrative Assistant

Natalie Stephens, M.Ed.
Coordinator

KATHRYN A. HEAD SCHOLARSHIP WINNER

In summer of 2018 the Kathryn A. Head Scholarship for McNair Scholars was awarded to two Scholars: Octavio Miranda, a Chemistry major mentored by Dr. Alejandro Bugarin, and Elida Sorto-Ramos, an Aerospace Engineewring major mentored by Dr. Haiying Huang. Octavio and Elida were selected for this award based on their outstanding letters of recommendation, application essay, academic achievement, and commitment to pursuing research and the professoriate.

The scholarship honors the long and exemplary career of Kathryn A. Head, former director of the McNair Scholars Program and SOAR Learning Services. The scholarship committee includes Natalie Stephens, McNair Coordinator; Dr. Shawn Christensen, Biology Professor and Graduate Advisor of Current Ph.D. Students; Jennifer Luken-Sutton, Director of Student Support Services Director and the I.D.E.A.S. Center; and Laura Wolf, Assistant Director of University Studies, now known as The Division of Student Success.

We thank our committee members for their commitment to selecting the best candidates for this honor, and we congratulate Octavio and Elida on receiving it.

FRIENDS OF THE UTA LIBRARY SCHOLARSHIP WINNERS

In November, the annual Friends of the UT Arlington Library McNair Scholarship was awarded to Ryne Dingler (Physics) and Regan Kubicek (Mechanical Engineering) for their McNair research presentations and papers.

The scholarship recipients are determined by the excellence of the Scholars' oral research presentations and papers, as assessed by members of the Friends McNair Scholarship Committee: Maggie Dwyer, Lorraine Levine, and William "Bill" Stallings. For the third year, the McNair Research Journal is online, with the technical and financial support of the UTA Library. The online version of the journal includes the four top-ranked papers, those by the two scholarship winners named above as well as Efret Ghirmazion (Nursing) and Paola Iracheta (Aerospace Engineering). All other McNair research interns share their results by having their abstracts published in the journal.

The McNair Scholars Program congratulates its 2018 scholarship winners and thanks the Dean of the Library, for their continued support.

From left to right: Regan Kubicek, Joan Reinhardt, and Ryne Dingler

McNair Papers

Volume 22 • 2018

McNair Scholars Research Journal
Vol. 22 • 2018
ISSN 2642-2492
doi:10.32855/mcnairscholarsuta.2018.001

MASSIVE STAR FORMATION IN THE INFRARED: A REANALYSIS OF THE SOMA SURVEY

RYNE DINGLER
DEPARTMENT OF PHYSICS

Faculty Mentor: Manfred Cuntz

ABSTRACT

Formation of massive stars ($M > 8\ M_{\odot}$) is a fundamental, yet not fully understood, process in galactic evolution. The universe is composed of elements forged through cosmological processes, many of which, especially heavy elements, are created, then released, by supernovae at the end of the evolution of massive stars. Consequently, a strong interdependence is displayed between the composition, distribution, and dynamics of the clump and envelope/core environments in star-forming regions (SFRs) and the birth, development, and death of massive stars. Many mathematical models have been generated to predict the initial mass of formed stars relative to the initial conditions of the star-forming areas; however, all models must make assumptions to fit observational results properly and do not fully explain environmental contribution in high mass stellar birth. The SOMA survey tests the astrophysical consistency of the adapted Turbulent Core Model of Zhang and Tan. In this research, previous observations from the Stratospheric Observatory for Infrared Astronomy (SOFIA) were further scrutinized for a better understanding of the connections between the factors that influence massive stellar formation. From this, we have revealed potential correlations or lack thereof, tendencies, and discrepancies amongst this data that provide further information for model adjustments.

Massive stars are unequivocally essential components in the chemical and physical development of galaxies, planetary systems, and ultimately the emergence of life. Their formation and development have been of steadily increasing interest among astrophysicists, biochemists, and exobiologists, as well as members of other fields. Generally, any main-sequence star with a mass higher than eight solar masses ($M_{\odot}$) is described as massive, containing a wide range of astrophysical roles and fates (Matteucci 2008). Though stars of these masses only compose $\lesssim 0.1\%$ of all stars, they contribute significantly to the chemical and astrophysical development of the universe (Powell 2006, Matteucci 2008). All stars conduct nuclear fusion in which elements, beginning with hydrogen, are fused together to form heavier elements. Consequently, the ability for stars to form elements of higher proton count increases with mass, essentially resulting in heavier elements from more massive stars (Matteucci 2008).

These elements, many of which are essential for life as we know it, are released into the interstellar medium (ISM) during and at the end of the star's life; the latter occurs through an explosion known as a supernova, which additionally generates super-heavy elements (Matteucci 2008, Winters 2016, Johnson 2017). To understand how vital massive stars are to us, we must look within ourselves and examine our composition. The six most essential elements of life are oxygen, carbon, hydrogen, nitrogen, calcium, and phosphorus (Winters 2016). Of these six, without massive stars, we would only have two or three in sufficient quantities; low mass stars are capable of the formation of carbon and nitrogen, while hydrogen was formed during the Big Bang (Johnson 2017). The process of nucleosynthesis during stellar evolution is mostly standard and well understood; it begins at the core with hydrogen, which fuses to helium, which in turn fuses to make carbon, and so on, with the core forming larger elements that push precursors farther out in layers (Rauscher & Patkos 2011). However, the extent of fusion is directly linked to the mass of the stars; a simplified view of the various mechanisms that facilitate nuclear fusion is illustrated in Figure 1 (Johnson 2017). Further fusion can be facilitated by explosive nucleosynthesis through proton and neutron capture or gamma burst irradiation that generates elements like Ca for the O/Ne shell or elements larger than Fe forming at the core to be released and potentially fused further when the star explodes (Rauscher & Patkos 2011).

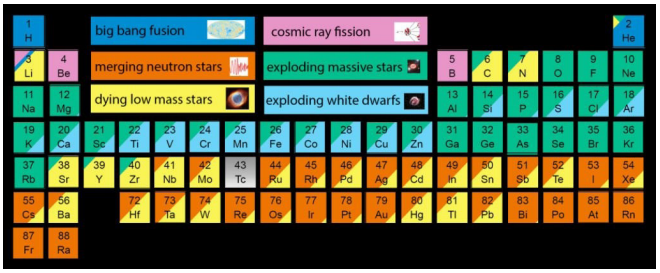

Figure 1. This figure displays the periodic table color-coded by the mechanisms of formation (Johnson 2017).

For us to exist, stars, huge ones at that, must die. The mass of the star determines not only the mass of elements generated but also the magnitude of supernovae and the resulting dispersion of stellar matter and energy, even blowing elements between galaxies if the explosion is powerful enough (Gibson et al. 2003, Matteucci 2008). As a result, a relationship presumably exists between the development and distribution of massive stars and the chemical composition and dynamics of ISM within star-forming regions (SFRs) (Gibson et al. 2003).

SFRs are domains of dense, opaque, turbulent gas gravitationally and energetically bound to nearby forming objects by accretion and outflow of matter and energy (Beuther et al. 2006, Motte et al. 2018). Within SFRs are clumps of gas that lead to the formation of stellar clusters and cores that form individual stars (Beuther et al. 2006). Recent observations and models have shown cores to have, typically, similar surface density to their clump (~ 1 g/cm^2), which provides for a high mass accretion rate, potentially necessary to form massive stars (Zhang et al. 2014).

New models of formation suggest these cores are spherical and self-gravitating around a protostellar object that has a rotating disk, which preserves angular momentum and provides pressure and energetic equilibrium that resists the fragmentation of the massive core into many smaller cores (Zhang & Tan 2011). This is illustrated in Figure 2. The accretion of matter onto

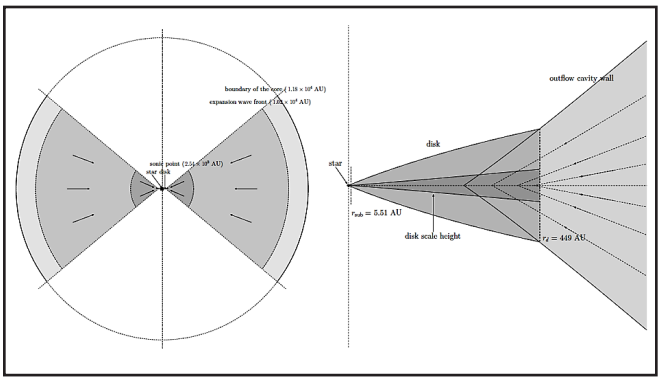

Figure 2. This figure illustrates the fiducial model of a developing protostellar structure (Zhang & Tan 2011). The left is a view of the core while the right displays a magnified view of the star and surrounding disk.

the protostar and disk drive the bipolar energetic outflow through the core into the clumps and neighboring areas (Zhang & Tan 2011, De Buizer et al. 2017). Consequently, these areas are most functionally observed utilizing infrared light produced by the excitation of gas by outflows (De Buizer et al. 2017). Due to the relatively "cool" temperatures of ISM within clumps and cores, infrared is an optimal segment of the electromagnetic spectrum in which to observe SFRs (Zavala & Yorke 2018 [iii]). This research will focus on the analysis of previous observations made by the Stratospheric Observatory for Infrared Astronomy (SOFIA), further discussed in the Materials and Methods section. Observations and models of the relative accretion and release of matter and energy in SFRs, especially those in which massive stars or protostellar objects are known, can be used to extrapolate vital factors that differentiate massive star formation (De Buizer et al. 2017). Herein lies one of the most significant issues of modeling the formation of massive stars. The influence of competing mechanisms involved in the formation of massive stars is not entirely understood (De Buizer et al. 2017). Many previous models do not account for the dense nature as well as the vast distance ($\gtrsim$ 1 kpc; ~ 3262 ly) of SFRs or clumps that result in the extinction of light at shorter wavelengths by optically thick cores and disks (Beuther et al. 2006, Zhang & Tan 2011, De Buizer et al. 2017). For each model developed in an attempt to describe the frequency, distribution, and mass of forming stars, there are remaining uncertainties and inconsistencies with observations (McKee & Tan 2002, Beuther et al. 2006, De Buizer et al. 2017). These are likely a result of the difficulties in observing such dense clumps and cores as well as a convoluted interdependency of model parameters, critical assumptions, and parameters per model (McKee & Tan 2002, Beuther et al. 2006, De Buizer et al. 2017). Current research also tends to lack significant connections between the development and distribution of heavy elements by massive stars and supernovae relative to the prediction of formation and distribution of massive stars (De Buizer et al. 2017).

In this research, we will focus on data from the SOFIA MAssive (SOMA) star formation survey developed by De Buizer et al. (2017), which is aimed at better describing the initial conditions that may influence massive star formation. This survey takes advantage of the lower density environments of outflow cavities to expand the infrared perspective of massive star formation and make predictions about initial conditions. Further analysis of data provided by this survey may provide clarity to vital factors and trends that influence massive star formation that may allow for future astrophysicists to better parameterize models and make adequate assumptions. Further discussion of the analysis of this paper and similar works will follow in the Materials and Methods section.

Materials and Methods

This research focuses on the further scrutinization of data collected by De Buizer et al. (2017). This survey was conducted using the SOFIA Mission, a partnered project between NASA and the German Aerospace Center, to collect high-resolution observations above most of Earth's interfering atmosphere (Gehrz et al. 2009, De Buzier et al. 2017, Zavala & Yorke 2018 [i]). SOFIA is a modified Boeing 747SP aircraft equipped with an infrared telescope with an array of instruments that provide observations in the infrared spectrum as well as improved sensitivity and spatial resolution over ground-based infrared telescopes (Zhang & Tan 2011, Zavala & Yorke 2018 [i]). Objects of interest in this study were observed at an altitude of ~39000 – 43000 ft (De Buizer et al. 2017). Observations using

SOFIA employ what is called the chop-nod technique in which the telescope moves up and down as well as back and forth at a slight angle such that a wider, more defined area can be observed (Zavala & Yorke 2018 [iv]). It is also equipped with the Faint Object infraRed CAmera for the SOFIA Telescope (FORCAST), which provides spectrographic information between ~5 and 40 micrometers (MIR) in wavelength (Zavala & Yorke 2018 [ii]). This instrument is composed of two separate cameras capable of observing wavelengths above or below 25 μm (Zavala & Yorke 2018 [ii]). Wavelengths within the mid-infrared range observed by FORCAST are readily associated with young stellar objects, which consequently allow for representative spectral energy distributions (SEDs) that describe celestial objects within SFRs (De Buizer et al. 2017).

De Buizer et al. (2017), with SOFIA and FORCAST, provide a multi-wavelength perspective of currently 8 out of an expected 50 protostars of interest. This study utilized a variety of observational filters for the most advantageous use of SOFIA's wide observable range, thus allowing for a more comprehensive mapping (near and far sides) of the objects and descriptions of their protostellar properties. It is speculated that the outflows from protostars have a significant effect on our observations by removing interfering gas, thoroughly reducing the absorption and scattering of light in those directions (De Buizer et al. 2017). Thus, the interconnection of bound ISM (core/envelope gas) and the high-velocity flow of matter from young stellar objects means that SEDs of outflow from protostars can predict initial conditions that led to the formation of massive stars (Beuther et al. 2006, De Buizer et al. 2017). Properties were estimated by fitting two competing accretion models to relative SEDs in thousands of simulations (De Buizer et al. 2017). Provided in the paper are eighty sets of mechanism parameters (2 models, 8 objects, 5 fits per object) corresponding to the best fit models. This study focuses on the forty results of the model developed by Zhang and Tan (2011) and Zhang et al. (2013, 2014).

The current SOMA survey does not provide data in a manner that are easily understood or comparable with each other. Data were further collimated and simplified through the generation of histograms and scatter plots to potentially reveal parameters of interest and significant trends or lack thereof while simultaneously providing a more understandable data reference. Parameters were also compared concerning each other to search for relative influence and interdependencies of physical and dynamic conditions. Results found are further discussed in context to influential parameters, potential reduction of uncertainty in future modeling, and the predicted astrophysical consequence.

Results

The radiative transfer model investigated by Zhang and Tan in this paper, as well as a series in preparation for this project, is a revision of the previous Turbulent Core Model (McKee & Tan 2002, 2003). This model is an improved version of scaled-up formation derived from the low-mass star model and aimed at connecting the accretion rate, core mass, surface density, and evolution (McKee & Tan 2002, De Buizer et al. 2017). This model was developed to resolve the contradiction between accretion and radiation pressure of previous models that would prevent the formation of massive stars; it is now physically consistent by accounting for the pressure from the density of gas surrounding the core and magnetic field interactions and stabilized angular momentum of disk in-falls and bipolar outflows (McKee & Tan 2002, Zhang et al. 2013, De Buizer et al. 2017). All parameters are derived by simulating and analyzing the SEDs from infrared observations of outflow cavities (De Buizer et al. 2017). Within the data shown below (Figures 3-9) are the 40 best fitting parameters derived for 8, Type II (hypercompact) young stellar objects (5 each) identifiable by the jet radio emission and far-extending MIR emission (De Buizer et al. 2017). This model derivation is limited to 3 parameter assumptions of core mass, clump density, and protostellar mass, though the use of a wide array of sampling resulting in 432 potential models compensates for these assumptions (De Buizer et al. 2017). Though limited by the efficiency of final stellar formation, this sampling method allows for various combinations of initial core parameters and specification of an evolutionary stage (De Buizer et al. 2017).

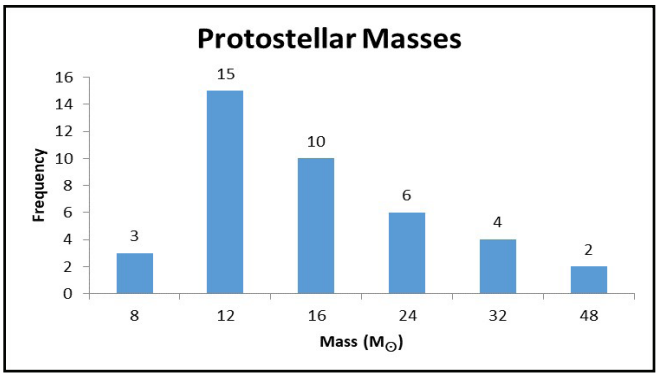

Figure 3. The figure above displays the sample of protostellar masses given as 0.5, 1, 2, 4, 8, 12, 16, 24, 32, 48, 64, 96, 128, and 160 $M_{\odot}$. This sample results in a mean mass of 18.3 $M_{\odot}$, with a median of 16 $M_{\odot}$. 37.5% of data result in masses 12 $M_{\odot}$ and 87.5% amongst 12 and 16 $M_{\odot}$.

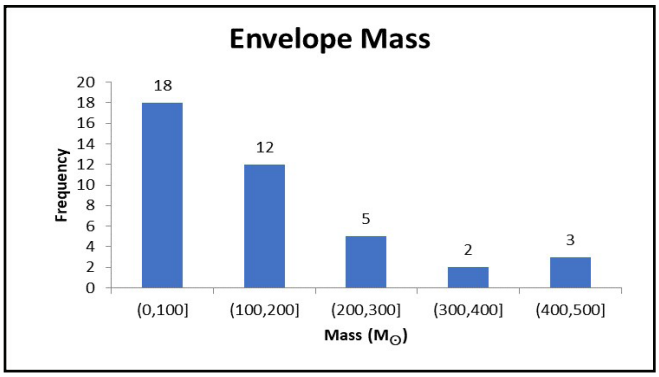

Figure 5. The figure above displays the derived envelope masses (gravitationally bound surrounding gas) from the sample. This displays a mean envelope mass of 156 $M_{\odot}$ with a median value of 130 $M_{\odot}$ and 75% of the sample within the range (0, 200] $M_{\odot}$.

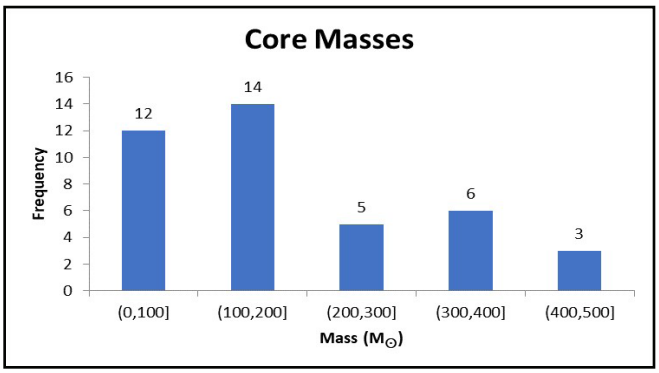

Figure 4.1. The histogram above displays the core masses utilized sampled at 10, 20, 30, 40, 50, 60, 80, 100, 120, 160, 200, 240, 320, 400, and 480 $M_{\odot}$. This sample resulted in a mean mass of 198.25 $M_{\odot}$ with a median of 160 $M_{\odot}$. A larger portion (35%) can be seen falling within [100, 200] $M_{\odot}$ with 65% falling between (0, 200].

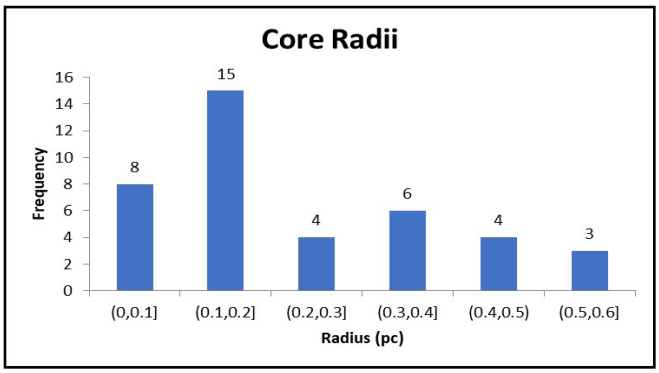

Figure 6. The figure above displays the core radii (pc) derived in this study. Core radii are a property defined by core mass and clump density samples. This sample has a mean radius of 0.23 pc and a median of 0.17 pc with 57.5% falling in a range of (0, 0.2] pc.

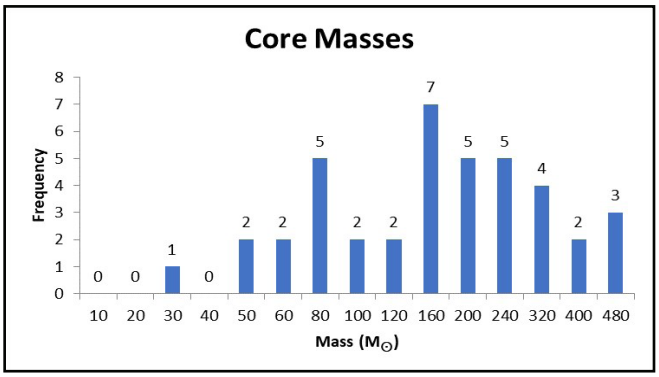

Figure 4.2. The histogram above displays the core masses utilized sampled at 10, 20, 30, 40, 50, 60, 80, 100, 120, 160, 200, 240, 320, 400, and 480 $M_{\odot}$. This sample resulted in a mean mass of 198.25 $M_{\odot}$ with a median of 160 $M_{\odot}$. A larger portion (35%) can be seen falling within [100, 200] $M_{\odot}$ with 65% falling between (0, 200].

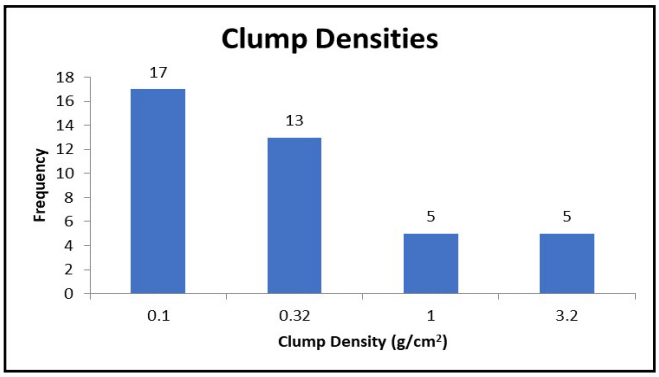

Figure 7. The figure above displays the clump densities utilized in SED analysis. This parameter was sampled at 0.10, 0.32, 1, and 3.2 g/cm^2. 75% of the sample can be observed to best fit with a density of either 0.1 or 0.32 g/cm^2, 42.5% to 0.1 g/cm^2 alone. This demonstrates a mean density of ~0.67 g/cm^2, with a median of 0.32 g/cm^2.

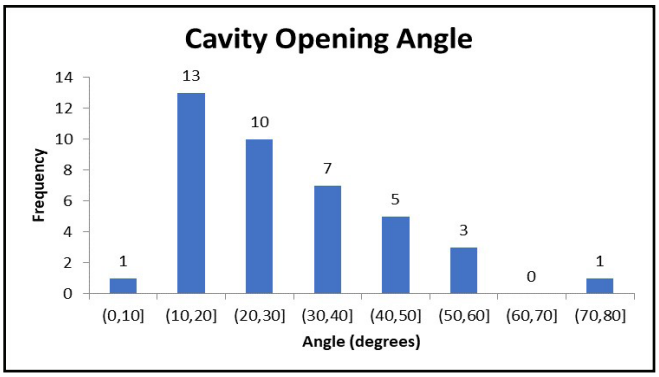

Figure 8. The figure above displays the opening angle of outflow cavities. We find in this sample an average opening angle of 30 degrees with 60% within [10, 30] degrees and a median value of 25.5 degrees. There can be observed a tendency for smaller opening angles within this data. This is likely a result of many models to reflect an early phase in the stellar evolution.

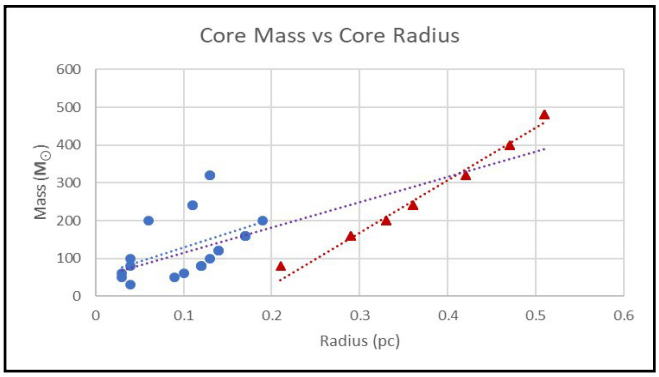

Radius < 0.2 Blue: $r^2 = 0.2007$
Radius > 0.2 Red: $r^2 = 0.9852$
All data Purple: $r^2 = 0.6568$

Figure 10. Shown above are potential relations between core mass and radius. From this, we find a weak positive correlation amongst the total data; when grouped, we find a strong positive correlation for radii > 0.2 pc and virtually no correlation for radii < 0.2 pc.

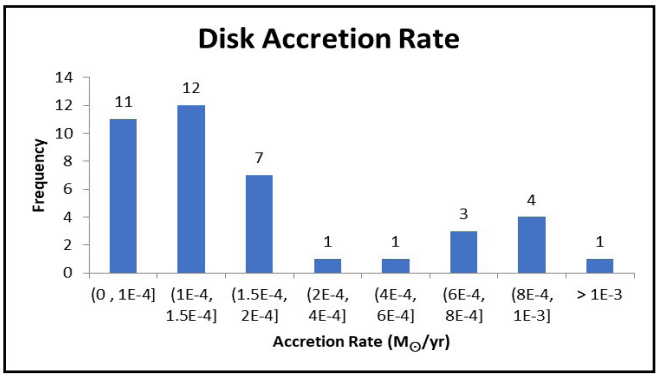

Figure 9. The figure above displays the derived disk accretion rates of the sample in $M_\odot$/year. The disk accretion rate may be an important factor in the stability of outflows and the resultant luminosity of the protostar. The mean disk accretion rate was found to be -2.9 × 10^{-4} $M_\odot$/yr and a median rate of 1.3 × 10^{-4} $M_\odot$/yr with 55% falling within (0, 1.5] × 10^{-4} $M_\odot$/yr. It is thought there are interdependencies between model parameters in this study. Here, we present a variety of comparisons (Figures 10-18) with the hope of revealing or deconvoluting potential parameter relations. Linear fits provide adequate comparisons for potential relations, and it is deemed unnecessary to attempt fits of a higher order. The value for the coefficient of determination is provided in the legend to the side of each figure to represent the fit from each comparison. The significance of correlation for is determined by reference to statistical literature (Hahn 1973).

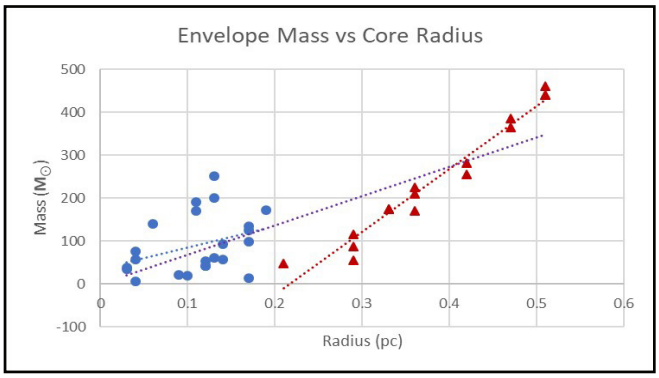

Radius < 0.2 Blue: $r^2 = 0.1282$
Radius > 0.2 Red: $r^2 = 0.9599$
All data Purple: $r^2 = 0.6751$

Figure 11. Shown above are potential relations between the envelope mass and core radius. From this, we find a weak positive correlation amongst the total data; when grouped, we find a strong positive correlation for radii >0.2 pc and virtually none for radii <0.2 pc.

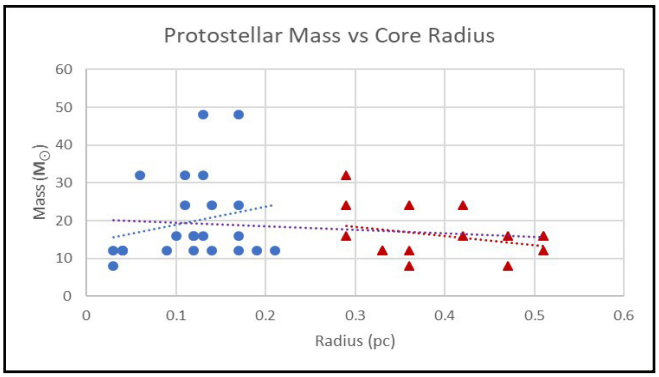

Radius < 0.2 Blue: $r^2 = 0.0523$
Radius > 0.2 Red: $r^2 = 0.0899$
All data Purple: $r^2 = 0.0213$

Figure 12. The figure above illustrates a comparison of protostellar mass to core radius. Data are grouped above and below a radius of 0.25 pc. No correlations are observed in this comparison.

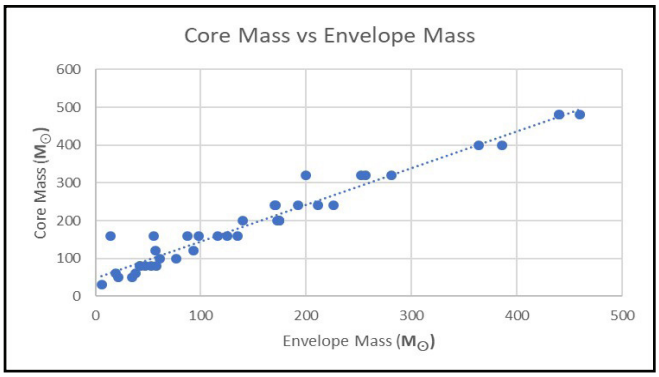

Blue: $r^2 = 0.9482$

Figure 14. The figure above illustrates a comparison of the core to envelope mass. This demonstrates a strong linear correlation such that we conclude envelope mass is a very good predictor of core mass with an almost 1:1 relation.

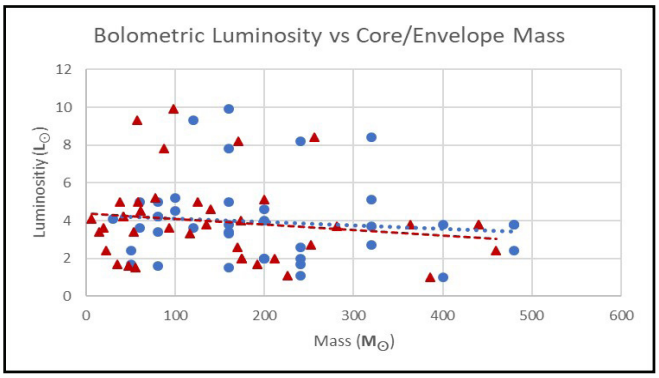

Core Mass Blue: $r^2 = 0.01$
Envelope Mass Red: $r^2 = 0.02$

Figure 13. Shown above are comparisons in an attempt to describe envelope mass as a predictor of luminosity. From this, we can say neither the envelope nor core mass can predict the luminosity.

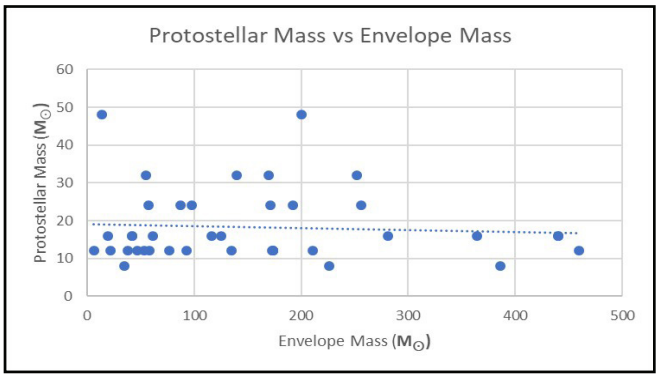

Blue: $r^2 = 0.0049$

Figure 15. Above is an attempted relation between protostellar and envelope mass; no correlation is demonstrated.

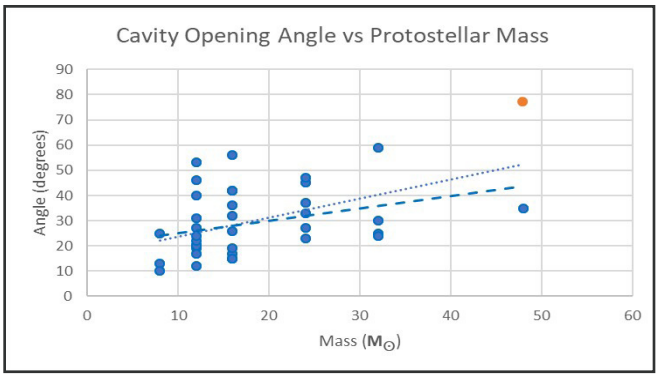

Total data Blue dotted: $r^2 = 0.2514$
Outlier Orange
Without outlier Blue dashed: $r^2 = 0.1075$

Figure 16. Shown above are comparisons in an attempt to describe protostellar mass as a predictor of cavity opening angle. There is virtually no correlation between these parameters. However, the correlation significantly depreciates if the outlier is disregarded.

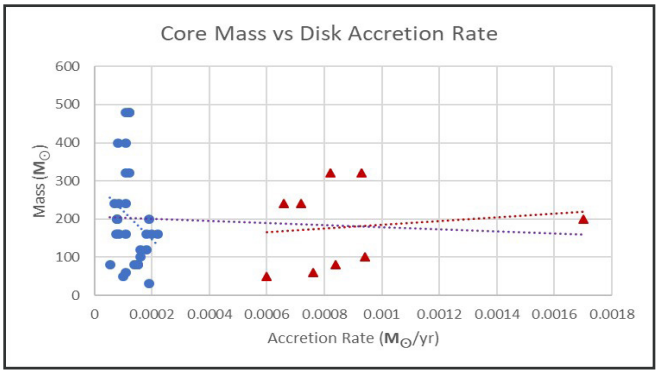

Rate < 5 Blue: $r^2 = 0.0631$
Rate > 5 Red: $r^2 = 0.0222$
All data Purple: $r^2 = 0.0059$

Figure 17. Shown above are attempted comparisons of core mass to accretion rate. Data are grouped above and below an accretion rate of 5 $M_\odot$/yr. No significant correlations are found amongst either data set.

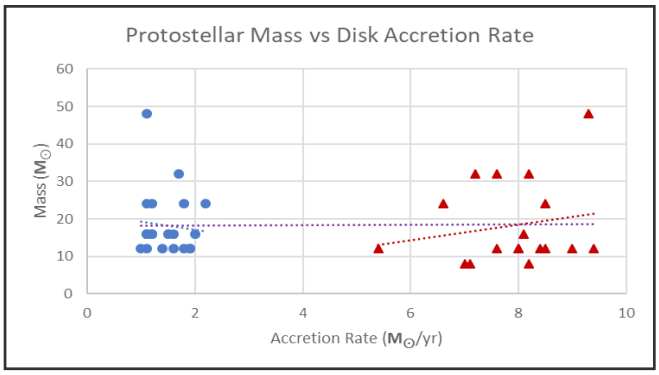

Rate < 5 Blue: $r^2 = 0.0082$
Rate > 5 Red: $r^2 = 0.0342$
All data Purple: $r^2 = 0.0003$

Figure 18. Shown above are attempted comparisons of core mass to accretion rate. Data are grouped above and below an accretion rate of 5 $M_\odot$/yr. We find no correlations amongst either data set.

Discussion

The SOMA survey utilizes a model developed by Robitaille et al. (2007) for the comparison of physical consistency against the turbulent core model of Zhang & Tan (2011) and De Buizer et al. (2017). This model was developed for prediction and modeling of low mass protostars but may be useful as well for comparison if massive stars form similarly, influenced primarily through the accretion of the core, envelope, and disk (Robitaille et al. 2007). However, unlike the model developed by Zhang and Tan (2011), which has only five free parameters, this model contains ~30 parameters, of which, only a few parameters similar to the previous are given (De Buizer et al. 2017). While not providing potential estimates of core mass and radius or clump surface density, this model does provide an estimation of envelope radius and accretion rate not given by Zhang & Tan (2011) and De Buizer et al. (2017). However, the first results of De Buizer et al. (2017), as well as further analysis, shows this data to be physically inconsistent and inconclusive. We thereby decided to exclude this data from further analysis at this time.

We have presented, in Figures 3-9, potentially interesting parameters of this survey. Some parameters (e.g., luminosity, viewing angle, etc.) are excluded

because they apparently do not contribute further to our understanding of massive star formation. Due to the differences in evolutionary stage amongst the sources, results may require further scrutinization in the context of the stage as well as an individual analysis of each source. We find amongst this sample a tendency for protostars to form at ~12-16 $M_\odot$(Figure 3) from cores of ~80-200 $M_\odot$ (Figure 4) and envelopes of similar size (Figure 5). This may require further analysis as formation efficiency (protostellar mass/core mass) is expected to be ~0.4-0.5, which we do not find from these results (Zhang & Tan 2011, De Buizer et al 2017). Over half the sample resulted in core radii within [0.1, 0.2] pc (Figure 6), the majority of which have surface clump densities of 0.1 g/cm^2 (Figure 7). Those objects that do not have a clump surface density of 0.1 tend to fall under the density of 0.32 g/cm^2 with only 10 results in the sample above this amount. This is contradictory to previous models that predict a mean clump surface density of ~1 g/cm^2 (McKee & Tan 2003, Zhang et al. 2014). The cavity opening angles vary amongst the sample, though a majority can be observed between 10 and 30 degrees (Figure 8). The disk accretion rate for this sample is found most to be 0.5-1.5 $M_\odot$/yr (Figure 9). The rate of disk accretion may be useful for extrapolating the mass of the disk which should be ~1/3 of the eventual protostellar mass (Zhang et al. 2014).

Figures 10-18 demonstrate a series of initial simple comparisons that explore simple direct correlations amongst two chosen parameters. This method may not be entirely insightful as many parameters may have more intricate relations that do not follow linear correlations or have multiple mutual dependencies not accounted for. Our first comparisons of core radius as a predictor of mass (Figure 10) show that the radius of the core can be a strong predictor of envelope and core mass above 0.2 pc (Figure 11) but displays no correlation for protostellar mass (Figure 12). Consequently, this may demonstrate that while the size of cores and envelopes may directly correlate to their masses, they show no inherent value in presuming the mass resultant protostar. It is expected that the mass of the core should be related to the radius, though the data reveals there may be a discrepancy in models of smaller radii. We also compare our values of core and envelope mass to test for a correlation to bolometric luminosity for which we find none (Figure 13). Main sequence stars of masses 0.43 $M_\odot \leq M \leq$ 20-55 $M_\odot$ should follow a relationship such that

$$\left(\frac{L}{L_\odot}\right) \propto \left(\frac{M}{M_\odot}\right)^{n(m)}$$

where $3 \leq n \leq 4$ and n decreases to ~ 1 as mass exceeds 55 $M_\odot$ (Harwit 1988, Salaris & Santi 2005, Thompson 2013). However, this study does not account for the full luminosity or mass of the final star but rather an integration of the flux from the observed outflow (De Buizer et al. 2017). Thus, we can suggest that one or more of these properties (likely the core and/or envelope mass) are not representative of the actual value and that core and envelope mass do not predict the final stellar mass. A comparison of envelope and core mass find a direct near 1:1 positive linear correlation (Figure 14). This may demonstrate the difference in density between the core and envelope. Presumably, the envelope encompassing the core should demonstrate a density similar to the clump environment such that

$$\Sigma = \frac{M}{\pi R^2}$$

(McKee & Tan 2002, Beuther 2006). From this, if the core and envelope masses are similar as observed, utilization of clump density may be a method of calculating and comparing the size or density of the core based on observation of clump densities and sizes of observed objects. A comparison of protostellar masses and envelope masses shows that the protostellar mass is distinct from that of the envelope (Figure 15). The similarity observed between the envelope and core mass means that the same can be said for the core mass. This result is unexpected because, as stated, previous model estimates predict a formation efficiency of ~0.4-0.5 from core to final protostar (Zhang et al. 2014). This may indicate a degeneracy in such estimates. We compared the protostellar mass against the angle of the cavity opening to identify a very weak correlation amongst the data. It was inferred one point was an outlier, so another comparison is shown without the

expected outlier to show virtually no relation (Figure 16). This is an expected outcome as the cavity opening angle is more closely a factor of the phase in the stars' evolution, not their mass. The accretion of the disk is essential for maintaining a pressure equilibrium amongst inflow and outflow of matter (Zhang et al. 2014). We thereby compare core and protostellar mass against the disk accretion rate (Figure 17). The large gap in the data has thereby provided for grouping of data above and below ~$5x10^{-4}$ $M_{\odot}$/yr. No correlation is observed for either groupings or the total data in either comparison. This may suggest that while the accretion disk may provide for pressure stability, the rate of its accretion has no significant effect on the mass of either the core or the final protostar (Figure 18).

We have thus demonstrated the initial phase of SOMA reanalysis. We have illustrated the current data in a manner to enhance comparability. Comparisons at this point have revealed some interesting trends and tendencies of the data set thus far. These tendencies may prove useful when adapting model parameters such that calculated and observed variations can be understood. Such comparisons will be necessary to adapt as the sample size of SOMA increases. Further research and analysis should include similar comparisons that group data sets according to internal parameters that may allow insight into the structure and dynamics during stellar formation.

Conclusion

In this paper, we have discussed the relative importance of massive stars in the chemical evolution of the universe not previously discussed in the SOMA survey. Again, it should be stated that the study of massive stars is of significant interest for galactic chemistry, planetary systems, and the origin and development of life. It is thus by defining how they formed that we can have a better understanding of what may define their distribution and potential "hot-spots" for massive stars within the universe. We have thereby further demonstrated the significance of reanalysis of modeling data and the importance of clear, resolute stratospheric observations done by SOFIA.

Our results have demonstrated some significant tendencies among parameters, such as the various resultant masses of core, envelope, and protostar, that appear to be independent of a source's point in evolution. This suggests that modeling of masses for either component can be used for a variety of forming protostars without direct influence from their evolutionary history. We have also identified several parameters that initially demonstrate no correlation. It is unclear whether relations do not exist; nevertheless, there may some "hidden" influential factor not considered. This result could, in fact, reveal potential issues or errors. For example, our results demonstrate no correlation amongst the envelope and core masses to the final protostellar mass, which was previously thought to be ~0.5; this is an important aspect deserving further attention.

Future expansion of this research aims to further analyze the increasing sample from the SOMA survey, which is expected to have ~50 sources by the end of summer in 2018. We also found that by grouping data sets within comparisons we might be able to further analyze the data in context to parameters influential in differentiating the environment and development during formation. Such properties include surface clump density, which could allow differentiating initial conditions on the variance of size and consequent pressure within the core and envelope, and cavity opening angle, which differentiates the samples based on evolutionary phase and outflow properties. Normalization may also be necessary to determine any correlations (if any) amongst parameters whose relations are more complex than investigated thus far. It may also be possible to extrapolate further properties to better define the pressure and temperature maps of the environment that leads to stars of a particular mass. In the future, with the increasing sample size of SOMA, it may be feasible to include a greater variety of conditions for comparison.

Acknowledgments

Thank you to Dr. Reinhardt and the McNair Scholars program for providing this research opportunity. Thanks also to Dr. Cuntz for his

guidance and mentorship. Appreciation to Dr. James De Buizer of SOFIA for his correspondence and work on which this analysis is based.

Works Cited

Beuther H., Churchwell E. B., McKee C. F., Tan J. C. 2006, De Buizer J. M., Liu M., Tan J. C., et al. 2017, ApJ, 834(1), 1-32

Gehrz R. D., Becklin E. E., de Pater I., et al. 2009, Adv. Space Res., 40(4), 413-432

Gibson B. K., Fenner Y., Renda A., et al. 2003, PASA, 20, 1-15

Hahn G. J. 1973, Chemtech, 3(10), 609

Harwit, M. 1988, Astrophysical Concepts, (2nd Ed.; Springer-Verlag, Berlin)

Johnson J. 2017, SDSS, http://blog.sdss.org/2017/01/09/origin-of-the-elements-in-the-solar-system/

Matteucci F. 2008, IAU Symposium, 250, 119

McKee C. F. & Tan J. C. 2002, Nature, 416, 59

McKee, C. F., & Tan, J. C. 2003, ApJ, 585, 850

Motte F., Nony T., Louvet F., et al. 2018, Nat Astron, doi: 10.1038/s41550_018_0452-x

Powell R. 2006. Atlas of the Universe, URL: http://www.atlasoftheuniverse.com/startype.html

Rauscher T. & Patkos A. 2011, Handb Nucl Chem, 611

Robitaille T. P., Whitney B. A., Indebetouw R., et al. 2007, ApJS, 169, 328

Salaris, M. & Santi C. 2005, Evolution of Stars and Stellar Populations, (John Wiley & Sons, Hoboken, NJ)

Thompson T. 2013, Introduction to Stars, Galaxies, and Cosmology, (Ohio State University, OH)

Winters M. 2016, WebElements, https://web.archiveorg/web/20160218020752/http://www.webelements.com:80/periodicity/abundance_humans/

Zavala E. & Yorke H. 2018, Sofia Science Center,
i. https://www.sofia.usra.edu/
ii. https://www.sofia.usra.edu/science/instruments/forcast
iii. https://www.sofia.usra.edu/public/about-sofia/science-behind-sofia
iv. https://sofia.usra.edu/science/sofia-overview/sofia-telescope

Zhang Y., & Tan J. C. 2011, ApJ, 733, 55

Zhang Y., Tan J. C., & McKee C. F. 2013, ApJ, 766, 86

Zhang Y., Tan J. C., & Hosokawa T. 2014, ApJ, 788, 166

McNair Scholars Research Journal
Vol. 22 • 2018
ISSN 2642-2492
doi:10.32855/mcnairscholarsuta.2018.002

THE EFFECTS OF POSTPARTUM DEPRESSION ON MATERNAL-INFANT BONDING AMONG MOTHERS EXPERIENCING A PRETERM BIRTH WITH NEONATAL INTENSIVE CARE ADMISSION

EFRET M. GHIRMAZION
DEPARTMENT OF NURSING

Faculty Mentor: Cheryl Anderson

ABSTRACT

A healthy maternal-infant bond is crucial for infant development and cognitive, social, and emotional development. Postpartum depression (PPD) places the developing bond between mother and infant at risk and can lead to bonding impairment. Phase 1 of this ongoing study aims to exam the prevalence of PPD symptoms and the relationship between PPD and maternal-infant bonding. To date eight mothers of premature infants completed the Edinburgh Postnatal Depression Scale (EPDS) and the Postpartum Bonding Questionnaire (PBQ). One mother displayed symptoms of mild depression (12.5%). A correlation between PPD and bonding scores was not found. A third research question to examine ethnic differences for PPD and bonding was not explored due to sample size. Early findings found the percentage of PPD at 12.5%, which reflects similar study findings for early postpartum mothers. Limitations include a small sample; further, timing of administration of the measurement tools may have influenced the results. Ongoing research, therefore, is important. Other researchers have recognized this potentially at-risk population, and because depression rates have been found to peak several months postpartum, practice implications include assessment of PPD and bonding at later postpartum, which will necessitate the involvement of agencies outside the hospital, for example, doctors' offices at well baby exams, to accomplish.

Postpartum depression (PPD) has increasingly been shown to be a major health problem affecting not only women but also their infants. Maternal depression prevents the formation of a strong maternal-infant bond, or attachment, and impairs a mother's ability to effectively and adequately care for her newborn. Mothers with PPD provide less stimulation to infants, are less responsive to infants, and show more parenting difficulties (Ertel, Rich-Edwards, & Koenen, 2011). Infants of depressed mothers are at high risk for delayed cognitive, language, and emotional development (Beck & Woynar, 2017). Further, the impact of PPD has been associated with poor outcomes beyond infancy, extending into childhood, adolescence, and adulthood (Mason, Briggs, & Silver, 2011).

Birth of a premature infant and hospitalization in a neonatal intensive care unit (NICU) have been recognized to associate with high rates of maternal aversive emotional states, including symptoms of acute stress, depression, and posttraumatic stress disorder (Andersen, Melvaer, Videbech, Lamont, & Joergensen, 2012; Jubinville, Newburn-Cook, Hegadoren, & Lacaze-Masmonteil, 2012). Infant prematurity as well as the physical separation of mother and infant due to NICU admission can lead to difficulty in establishing a mother-infant bond, and may further jeopardize maternal mental health. (Anderson & Cacola, 2017; Jubinville et al., 2012; Mason et al., 2011).

Postpartum depression is a global concern, with one epidemiological study reporting increasingly high rates of PPD in diverse cultures across the world (Rahman, Iqbal & Harrington, 2003). Determining the prevalence of PPD and its social and biological correlates across different populations and cultures is of importance in order to provide best practice (Wolf, Andraca, & Lozoff, 2002). A review of 143 studies identified a prevalence of PPD across 40 countries ranging from almost 0% to almost 60% (Halbreich & Karkun, 2006). In some countries like Singapore, Malta, Malaysia, Austria, and Denmark there are very few reports of PPD; whereas, in other countries such as South America and East Asia PPD symptoms are very prevalent (Zubaran, Schumacher, Roxo, & Foresti, 2010). The variability in reported PPD might be due to cross-cultural variables, differences in perception of mental health and resulting stigma, differences in socio-economic environments, and biological vulnerability factors (Halbreich & Karkun, 2006).

In the United States, childbearing women are of a mix of many cultures and backgrounds. Research has shown that racial/ethnic differences or one's culture may influence the rate of PPD. Liang, Matheson, and Douglas (2016) discussed several issues leading to a misdiagnosis of depression believed to occur owing to racial/ethnic differences regarding how a mental health condition is tolerated, how symptoms are expressed, or whether a mental health issue is believed to be pathological. The importance of culturally sensitive assessments is essential.

Racial/ethnic differences also are linked to adverse infant outcomes such as preterm birth, which has been recognized to occur among Black women at a higher rate than among White women. Illustrating the longstanding disparity between Black-White racial/ethnic groups in the United States, the most recent (2016) issue of the National Vital Statistics Reports indicated prevalence rates for preterm births at 13.7% for Black women versus 9.04% for White women (Martin, Hamilton, Osterman, Driscoll, & Drake, 2018). However, a national rate at 9.85% (up from 2015) shows the vulnerability of many women to experience a preterm birth, with the potential for ensuing depression and poor maternal-infant bonding.

Because of the prevalence of preterm births in the United States and the lifelong adverse effects of PPD on mothers and infants, it is imperative that an effective intervention for this potentially vulnerable cohort of women is identified. Despite statistics, however, intervention research aimed at the reduction of infant developmental delays and improved maternal mental health and maternal-infant bonding is lacking. Therefore, the purpose of Phase 1 of this ongoing, two-phase, longitudinal study is two-fold: 1) to examine the prevalence of PPD and the relationship between PPD and maternal-infant bonding among a group of ethnically diverse mothers who experienced a preterm birth with NICU placement, and 2) to determine the racial/ethnic impact on depression rates and bonding. Our purpose for Phase 2 research (not presented here) is to test the effectiveness of a novel interactional, home-based intervention aimed at reducing infant developmental delays among premature infants

and to improve maternal mental health status and maternal-infant bonding. Information obtained from this study is critical for future research, policy, and future intervention activities aimed at promoting the well-being of all mothers and infants.

To receive the intervention, infants must be a minimum of three months corrected age; therefore, at present, Phase 2 of the study has not begun. The presented study here describes preliminary data from Phase 1 of the study only.

Literature Review

Depression

In a review of 16 longitudinal studies, Underwood, Waldie, D'Souza, Peterson, and Morton (2016) found 13% of women experienced PPD. An individual study among a sample of Canadian women (N=308) over 18 (age mean 32) found slightly higher rates of PPD at 16.4% (Verreault et al., 2014). Depression rates, however, can be greatly increased among mothers of premature infants. In a systematic review of 59 studies, prevalence rates for depression were almost doubled among at-risk (14.1%) samples versus community samples (9.4%; Dikmen-Yildiz, Ayers, & Phillips, 2017). Significant symptoms of depression, sustained up to one month postpartum, have been found in 43% of mothers reporting a preterm birth (Jubinville et al., 2012). Further, in a separate study, over one-third of mothers with NICU infants were found to experience suicidal thoughts as compared to 14% of perinatal mothers in the general population (Lindahl, Pearson, & Colpe, 2005).

The connection between depression and preterm birth has been found by some researchers to be circular, in that depression prenatally may lead to the birth of a preterm infant (Grote et al. 2010), which then may produce symptoms of depression. Underwood et al. (2016) found the average rate for prenatal depression (17%) to be higher than that found at postpartum. A systematic review of 29 studies conducted by Grote et al. (2010) concluded that women with depression during pregnancy were at increased risk for a preterm birth. Yonkers et al. (2014) reported that women with major depression and PTSD were at a 4-fold increase for preterm birth. Further, report of depressive symptoms during the third trimester of pregnancy has been found to be a significant risk factor for lowered maternal-infant attachment (Banti et al., 2011). The importance of assessing depression symptoms during pregnancy is essential to best practice (Mason et al., 2011).

Ongoing assessment for mother and infant postpartum is also needed. Premature infants are at increased jeopardy for developmental delays because of their gestational age; further, birth of a premature infant can lead to poor maternal mental health (Anderson & Cacola, 2017). Infant development delays are in turn reinforced due to a depressed mother's lack of stimulation and responsiveness to her infant, and these conditions potentially set the stage for subsequent poor quality bonding.

Maternal-Infant Bonding

Mother-infant bonding is significant because it epitomizes a mother's maternal feelings about her infant and the subsequent developing emotional connection between the two. Bonding has a vital component to all aspects of infant well-being and is influenced by physical contact between the mother and infant. This long-term emotional attachment begins with the first contact between the mother and the infant (Figueiredo, Costa, Pacheco, & Pais, 2009). Mothers respond more affectionately to their infants with continuous contact and interaction; further, bonding appears to develop gradually, rather than being completely present at birth. Maternal bonding involves the participation of both the mother and the newborn. Infant behaviors, such as crying, eye contact, and facial expressions improve maternal attachment and aid in mutual emotional involvement (Figueiredo et al., 2009).

The mother's health and emotions, however, significantly contribute to the maternal-infant bond. The quality of the bond can be altered by various factors, some related to the infant, such as prematurity or physical disability, and others characteristic of the mother, including her support system, her style of attachment, physical illness, postpartum depression, or other mental health issues (Bienfait et al., 2011). Studies have shown that first-time mothers and women who experienced difficult labors involving severe pain, displayed less interaction and engagement with their newborns in the postpartum period (Figueiredo et

al., 2009). Other women following a caesarean birth, or receipt of epidural anesthesia have been seen to show a negative reaction to their infants and delay in care for the newborn (Figueiredo et al., 2009).

Racial/Ethnic Influence

Nunes and Phipps (2013) conducted a retrospective cohort study using state pregnancy risk assessment data (N= 3798) and found race to be a significant risk factor for PPD among adults. In addition, for Black women, a higher risk for preterm birth was found to remain even after adjustment for socioeconomic factors (Yee, Liu, Sakowicz, Bolden, & Miller, 2016). Therefore, because of potentially high depression rates and recognized higher rates of preterm births among certain racial/ethnic groups, research and practice attention should be focused on racial/ethnic influences. With recognition that depression can result in delayed infant development and poor quality bonding and that insecure maternal-infant bonding has been linked to poor mental health outcomes across ethnic populations, it is important to begin to identify the factors that are involved across and within different racial/ethnic groups (Anderson & Cacola, 2017; Perry, Ettinger, Mendelson, & Le, 2011) to implement and evaluate potentially effective interventions to improve maternal-infant outcomes.

With the given recognition of the importance of depression on maternal-infant bonding to the health of mothers and babies, the research questions of Phase 1 study are as follows:

1) What is the prevalence of PPD among ethnically diverse mothers with infants in NICU?

2) Is there a correlation between PPD and maternal-infant bonding in mothers with infants in NICU?

3) Does ethnicity impact PPD and maternal-infant bonding of mothers with infants in NICU?

Methods

The current study is part of an ongoing longitudinal study across 18 months. The study population consists of mothers of premature infants (defined as 37 weeks gestational age and below) admitted into NICU at John Peter Smith Hospital in Fort Worth, Texas. Women meeting specific inclusion criteria were approached to participate in the study. Criteria included an 18-year age minimum and ability to speak/read English or Spanish. Due to the setting (the county hospital), the majority of the women were of low education and income. Infants also met specific inclusion/exclusion criteria: gestational age of 37 weeks gestation or below, singleton birth, and without congenital abnormalities or anticipating surgery within the weeks following. Infants remaining in the NICU over three months were also ineligible for the study due to the timing of the intervention and first home visit for Phase 2 research. Preliminary work presented here is based on the comments of the first eight recruited mothers.

Assessments for depression were done in the NICU using the Edinburgh Postnatal Depression Inventory (EPDS; Cox, Holden, & Sagovsky, 1987). The EPDS is a 10-item self-report screen for depression. Responses are scored 0, 1, 2, and 3 according to the increased severity of the symptoms, with a total possible score of 30. According to Cox et al. (1987) an EDPS score for minor depression equals 10-12; above 12 signifies major depression. Recent refinements of the EPDS have suggested a score of 19 to indicate severe depression symptoms (McCabe-Beane, Segre, Perkhounkova, Stuart, & O'Hara, 2016). The EPDS has shown adequate reliabilities among multicultural and multiethnic populations. A split-half reliability of 0.88 and alpha coefficient of 0.87 have been noted (Venkatesh, Zlontnick, Triche, Ware, & Phipps, 2014). Convergent validity has been reported with the DSM-IV. Venkatesh, Zlotnick, Triche, Ware, and Phipps (2014) reported sensitivities of 90% and specificities of >85%.

The Postpartum Bonding Questionnaire (PBQ; Brockington et al., 2001) was used to determine bonding between the mother and infant. The PBQ is a self-rating assessment designed to detect disorders with the mother and infant relationship. The tool consists of 25 questions on a 6-point Likert scale. The scoring ranges from always (score 0) to never (score 5) with low scores indicating good bonding. The PBQ has four subscales to: reflect impaired bonding (scale 1), rejection and anger (scale 2), anxiety about care (scale 3), and risk of abuse (scale 4). A total score of over 36 reflects impaired

bonding. The PBQ has acceptable reliability and validity and extensive use in the childbearing population.

A third questionnaire collected demographic information such as maternal and gestational age, racial/ethnic identity, education level, and income. The completion of all questionnaires took approximately 40 minutes.

Data Collection

The aim of Phase 1 of this ongoing research study is 1) to assess the prevalence of depression symptoms and determine the relationship between depression and maternal-infant bonding of mothers with NICU admitted premature infants, and 2) to determine the racial/ethnic impact upon depression rates and bonding. Research team members approach mothers who meet age and language requirements of preterm infants (who also met specific eligibility requirements) with a description of the study and inquiry for participation. Following initial maternal eligibility and consent, research team members administer questionnaires in the NICU. The completion of questionnaires will provide data that serves as a pre-screen for additional eligibility into the study, and an early determination of mental health status, maternal-infant bonding, and potential need for referrals/resources; therefore, questionnaires are scored upon completion. Scores on the EPDS signifying a severe degree of symptoms (>19) or suicidal thoughts require a direct referral to in-hospital resources and ineligibility for the study. Total scores above 36 on the PBQ does not prevent enrollment in the study but suggests impaired bonding, and education and resources to the mother from NICU and/or postpartum nurses in person or via phone follow-up is required. Administration of the EPDS is done within three days postpartum, as possible, to determine need for referrals/resources as well as study eligibility. However, because of the possibility of "baby blues" early in postpartum, the EPDS is also re-administered at 10 days. Ideally, the PBQ is to be administered after one week, as possible, to allow some time for development of interactions between mother and infant. For the entirety of the 18-month study, assessments of maternal mental health and bonding are to be repeated.

For the preliminary data, analysis included the use of descriptive statistics, ANOVA to look for differences between variables of interest, and Pearson's Correlation coefficient to test for associations. All data was analyzed using SPSS version 23.

Results

Data on eight mother-infant dyads meeting the inclusion-exclusion criteria were available for the current analysis. Descriptive statistics inclusive of frequencies, percentages, means, and standard deviations identified the characteristics of mothers and infants as well as prevalence of depression and scores for the EPDS and the PBQ. The mean age of mothers was 25.6 (SD=4.89). Most were Black (n=4) and indicated a lower income and educational status with a mean grade level less than high school completion (11.7; SD=.487). Half were married. The majority did not work outside the home (n=6). Mothers typically reported a planned pregnancy and 75% indicated this current infant as their first-born. None of the mothers (n=5) reported a previous infant admitted into NICU. Five out of seven mothers had a cesarean birth; gestational age of infants averaged 31.87 weeks (SD=4.48; Table 1).

One mother showed current symptoms of PPD (12.5%). Depression histories varied between the mothers with one mother reporting depression symptoms before pregnancy, two mothers with prenatal depression, and one mother diagnosed with PPD previously. Two mothers reported being treated for symptoms, but no mothers reported current depression medication.

PBQ scores did not indicate impaired bonding with mean and median scores identical 3.50 (SD=2.73). Further, no correlation was noted between PBQ and EPDS scores. However, of interest, independent effects by both race/ethnicity, p=.037, and EPDS, p=.08, scores were noted on PBQ scores. An analysis was done to show only preliminary trends and caution with any findings at this stage is warranted due to very small sample size.

	Quantity	Percentage
Age, years		
18-24	3	37.5%
25-35	5	62.5%
Ethnicity		
White	1	16.7%
Black or African American	1	16.7%
Hispanic or Latino	4	66.7%
Asian or Pacific Islander	0	0.0%
Level of Education		
Did not complete high school	2	28.6%
High school diploma	5	71.4%
Associates degree	0	0.0%
Bachelor's degree	0	0.0%
Master's/Doctoral degree	0	0.0%
Marital Status		
Single	4	50%
Married	4	50%
Work outside home		
No	6	75.0%
Yes	2	25.0%
Planned Pregnancy		
No	1	14.3%
Yes	6	85.7%
Number of kids		
1 child	6	75.0%
> 1 child	2	25.0%
Birth Type		
Cesarean	5	71.4%
Vaginal	2	28.6%
Complications in Pregnancy		
No	2	25.0%
Yes	6	75.0%
Gestational Age		
24-28 weeks	2	25.0%
29-33 weeks	3	37.5%
34-37 weeks	3	37.5%
Infant weight (g)		
600-1200	1	14.3%
1201-1800	2	28.6%
1801-2000	1	14.3%
2001-2800	3	42.9%
Signs and symptoms of depression in the past		
No	6	75.0%
Yes	2	25.0%
Diagnoses of depression in the past		
No	4	80.0%
Yes	1	20.0%
Diagnoses of postpartum depression		
No	4	80.0%
Yes	1	20.0%
Medications for depression before		
No	5	71.4%
Yes	2	28.6%

Table 1. Sample Characteristics

Discussion

This is an ongoing two-phased longitudinal study across 18 months. The current data is limited to preliminary findings from a small sample of eight women; therefore, the following considerations are provided. The prevalence of PPD was found to be 12.5%, which is in line with other studies of PPD (Underwood et al, 2016) but below that found by other researchers for at-risk samples (Dikmen-Yildiz et al., 2017). A

later time for the depression assessment may show increased symptoms linked to the preterm birth and NICU admission. Jubinville et al. (2012) reported 43% of mothers with preterm infants in NICU had depression symptoms when surveys were administered between 7 and 10 days postpartum. Depression symptoms postpartum have been found to peak at three months (Gavin et al. 2005). With the shock of such traumatic birth events still present at 2-3 days postpartum, accuracy in surveys may be faulty, and attention to personal feelings may be superseded by feelings attached to the infant. Interestingly, the one mother scoring 10 on the EPDS (minor depression) omitted all questions related to past depression on her survey.

Symptoms of depression have been found to impact maternal-infant bonding (Anderson & Cacola, 2017); however, our lack of finding an association between these variables is most likely due to the small sample or timing of the administration of the measurement tool. Most bonding tools garner the most accurate information when mother and infant have had time to get acquainted, often administered at one month postpartum or later. Bonding appears to develop gradually, rather than being completely present at birth. The preliminary assessment of bonding is very early and hindered by the newborn's immediate level of care, and events ongoing in the NICU, perhaps, prohibiting mother-infant interactions and development of a bond.

Due to the small sample, differences in ethnicities were not analyzed. Some thoughts related to race/ethnicity and practice may be suggested given our population was mostly minority mothers recruited in a setting predominately Hispanic, but are not conclusions of the analysis. Health care providers should not stereotype postpartum women on the basis of their racial/ethnic background; rather, they should explore the cultural milieu (including education) of the patient beyond ethnicity and race. Postpartum mothers with lower levels of education may not disclose symptoms that usually trigger medical attention, such as crying and thoughts of self-harm. Further, some lower educated mothers may have difficulty discerning if symptoms experienced are related to normal pregnancy or perinatal depression (Recto & Champion, 2107). In cases involving at-risk mothers, health care providers may best be advised to focus on the presence of anhedonia and sensitively investigate other symptoms that may be present but not disclosed because of a perceived stigma (Di Florio, Putnam, Altemus, Apter, & Bergink, 2017).

Limitations

This ongoing research study provides early, preliminary data only. With only eight participants, we could not capture the true prevalence of PPD, its relationship with maternal-infant bonding, or the role of various ethnicities and cultures. An additional limitation is that mothers and infants differed in medical severity, including maternal concerns and infant concerns, such as gestational age; hence, their admission in the NICU and health progress trajectories varied. Further, mothers who chose not to participate in the study often cited strong family and partner support as a reason, possibly suggesting a difference in feelings in those mothers who did accept the study invitation. Lastly, timing of the administration of surveys prevented us from seeing beyond a possible pattern of symptoms; however, this information does serve as baseline data to be compared with survey data when re-administered to mothers periodically across Phase 1 and Phase 2 research.

Conclusion

This study provided some preliminary information on PPD and its relationship to bonding. It is important to be aware of life stressors, such as depression and preterm birth, and the possible impact upon the maternal-infant relationship, in order that interventions be tested and offered to reduce depression and facilitate mother-infant bonding. Research supports continued longitudinal study. Other researchers have recognized this population as potentially at risk, and continued monitoring of depression and assessment of maternal-infant bonding at a later postpartum time is essential but requires the involvement of agencies outside the hospital to accomplish, for example, at doctors' offices during well baby exams. A more complete understanding of the factors that impact maternal-infant bonding may

lead to improved health outcomes for mothers, infants, and families through identification of at-risk mothers and the provision of high-quality targeted interventions.

References

Anderson, C., & Cacola, P. (2017). Implications for preterm birth for maternal mental health and infant development. MCN, The American Journal of Maternal Child Nursing, 42(2):108–114. doi:10.1097/NMC.0000000000000311

Andersen, L. B., Melvaer, L. B., Videbech, P., Lamont, R. F., & Joergensen, I. S. (2012) Risk factors for developing post-traumatic stress disorder following childbirth: A systematic review. Acta Obstetrics Gynecology Scandinavia, 91, 1261–1272. doi:10.1111/j.1600-0412.2012.01476.x

Banti, S., Mauri, M., Oppo, A., Borri, C., Rambelli, C., Ramacciotti, D., Montagnani M. S., Camilleri, V., Cortopassi, S., Rucci, P., & Cassano, G. B. (2011). From the third month of pregnancy to one year postpartum, prevalence, incidence, recurrence, and new onset of depression. Results from the perinatal depression-research and screening unit study. Comprehensive Psychiatry, 52, 343–351. doi:10.1016/j.comppsych.2010.08.003

Beck C., & Woynar J. (2017). Posttraumatic stress in mothers while their preterm infants are in the newborn intensive care unit: A mixed research. Advances in Nursing Science, 40(4), 337–355. doi:10.1097/ANS.0000000000000176

Bienfait, M., Maury, M., Haquet, A., Faillie, J., Franc, N., Combes, C., Daude H., Picaud, J. C., Rideau, A., & Cambonie, G. (2011). Pertinence of the self-report mother-to-infant bonding scale in the neonatal unit of a maternity ward. Early Human Development, 87(4), 281–287. doi:10.1016/j.earlhumdev.2011.01.031

Brockington, I. F., Oates, J., George, S., Turner, D., Vostanis, P., Sullivan, M., Loh, C. C., & Murdoch, C. (2001). A screening questionnaire for mother-infant bonding disorders. Archives of Women's Mental Health, 3, 133–140.

Cox, J. L., Holden, J. M., & Sagovsky, R. (1987). Detection of postnatal depression: Development of the 10-item Edinburgh postnatal depression scale. British Journal of Psychiatry, 150, 782–786.

Di Florio, A., Putnam, K., Altemus, M., Apter, G., & Bergink V. (2017). The impact of education, country, race, and ethnicity on the self-report of postpartum depression using the Edinburgh postnatal depression scale. Psychological Medicine, 47(5), 787–799. doi:10.1017/S0033291716002087

Dikmen-Yildiz, P. D., Ayers, S., & Phillips, L. (2017). The prevalence of posttraumatic stress disorder in pregnancy and after birth: A systematic review and meta-analysis. Journal of Affective Disorders, 208, 634–645. doi:doi.org/10.1016/j.jad.2016.10.009

Ertel, K. A., Rich-Edwards, H. W., Koenen, K. C. (2011). Maternal depression in the United States: Nationally represented rates and risks. Journal of Women's Health, 20(11), 1609–1617.

Figueiredo, B., Costa, R., Pacheco, A., & Pais, A. (2009). Mother-to-infant emotional involvement at birth. Maternal & Child Health Journal, 13(4), 539–549. doi:10.1007/s10995-008-0312-x

Gavin, N. I., Gaynes, B. N., Bradley, N., Lohr, K. N., Meltzer-Brody, S., Gartlehner, G., & Swinson. T. (2005). Perinatal depression: A systematic review of prevalence and incidence. Obstetrics and Gynecology, 106, 1071–1083.

Grote, N. K., Bridge, J. A., Gavin, A. R., Melville, J. L., Iyengar, S., & Katon, W. J. (2010). A meta-analysis of depression during pregnancy and the risk of preterm birth, low birth weight, and intrauterine growth restriction. Archives General Psychiatry, 67, 1012–1024.

Halbreich, U., & Karkun S. (2006). Cross-cultural and social diversity of prevalence of postpartum depression and depressive symptoms. Journal of Affective Disorders, 91(2), 97–111. https://doi.org/10.1016/j.jad.2005.12.051

Jubinville, J., Newburn-Cook, C., Hegadoren, K., & Lacaze-Masmonteil, T. (2012). Symptoms of acute stress disorder in mothers of premature infants. Advances in Neonatal Care, 12, 246–253.

Liang, J., Matheson, B. E., & Douglas, J. M. (2016). Mental health diagnostic considerations in racial/ethnic minority youth. Journal of Child Family Studies, 25, 1926–1940. doi:10.1007/s10826-015-0351-z

Lindahl, V., Pearson, J. L., & Colpe, L. (2005). Prevalence of suicidality during pregnancy and the postpartum. Archives of Women's Mental Health, 8(2), 77–87. doi:10.1007/S00737-005-0080-1

Martin, J. A., Hamilton, B. E., Osterman, M. J., Driscoll, A. K., & Drake, P. (2018). Births: Final data of 2016. National Vital Statistics Reports, 67(1). Hyattsville, MD: National Center for Health Statistics. Retrieved from Centers for Disease Control and Prevention: https://www.cdc.gov/nchs/data/nvsr/nvsr67/nvsr67_01.pdf

Mason, Z. S., Briggs, R. D., & Silver, E. J. (2011). Maternal attachment feelings mediate between maternal reports of depression, infant social-emotional development and parenting stress. Journal of Reproductive & Infant Psychology, 29, 382–394. doi:10.1080/02646838.2011.629994

McCabe-Beane, J. E., Segre, L., Perkhounkova, V., Stuart, S., & O'Hara. M. (2016). The identification for severity ranges for the Edinburgh postnatal depression scale. Journal of Reproductive & Infant Psychology, 34, 293–303. doi:10.1080/02646838.2016.1141346

National Vital Statistics Reports. (2016). Center for Disease Control and Prevention, 65(2), 2-15.Perry, D. Ettinger A., Mendelson, T., & Le, H. (2011). Prenatal depression predicts postpartum maternal attachment in low-income latina mothers with infants. Infant Behavior and Development, 34(2), 339-350.

Nunes, A. & Phipps, M. (2013). Postpartum depression in adolescent and adult mothers comparing prenatal risk factors and predictive models. Maternal and Child Health Journal, 17(6), 1071-1079. doi: 10.1007/s10995-012-1089-5

Rahman, A., Iqbal, Z., & Harrington, R. (2003). Life events, social support and depression in childbirth: Perspectives from a rural community in the developing world. Physiological Medicine, 33(7), 1161–1167.

Recto, P., & Champion, J. D. (2017). Assessment of mental health literacy among perinatal Hispanic adolescents. Issues in Mental Health Nursing, 38, 1030–1038. doi:10.1080/01612840.2017.1349224

Underwood, L., Waldie, K., D'Souza, S., Peterson, E. R., & Morton, S. (2016). A review of longitudinal studies on antenatal and postnatal depression. Archives of Women's Mental Health, 19, 711–720. doi:10.1007/s00737-016-0629-1

Venkatesh K., Zlotnick, C., Triche, E., Ware, C., & Phipps, M. (2014). Accuracy of brief screening tools for identifying postpartum depression among adolescent mothers. Pediatrics, 133(1), 45-53. Verreault, N., Da Costa, D., Marchand, A., Ireland, K., Dritsa, M., & Khalif, S. (2014). Rates and risk factors associated with depressive symptoms during pregnancy and with postpartum onset. Journal of Psychosomatic Obstetrics & Gynecology, 35(3), 84–91.

Wolf, A., Andraca, I., & Lozoff, B. (2002). Maternal depression in three Latin America samples. Social Psychiatry and Psychiatric Epidemiology, 37(4), 169–176.

Yee, L. M., Liu, L. Y., Sakowicz, A., Bolden, J. R., & Miller, E. S. (2016). Racial and ethnic disparities in the use of 17-alpha hydroxyprogesterone caproate for prevention of preterm birth. Journal of Obstetrics & Gynecology, 214(3), 374e1–6. doi:10.1016/j.ajog.2015.12.054

Yonkers, K.A., Smith, M. V., Forray, A., Epperson, N., Costello, D., Lin, H., & Belanger, K. (2014). Pregnant women with posttraumatic stress disorder and risk of preterm birth. Journal of American Medical Association Psychiatry, 71(8), 897–904. doi:10.1001/jamapsychiatry.2014.558

Zubaran, C., Schumacher M., Roxo, M. R., & Foresti, K. (2010). Screening tools for postpartum depression: Validity and cultural dimensions. African Journal of Psychiatry,13(5), 357–370.

McNair Scholars Research Journal
Vol. 22 • 2018
ISSN 2642-2492
doi:10.32855/mcnairscholarsuta.2018.003

ANALYSIS AND DESIGN OF FAST-RESPONSE, RESISTANCE TEMPERATURE DETECTOR

PAOLA M. IRACHETA
DEPARTMENT OF MECHANICAL AND AEROSPACE ENGINEERING

Faculty Mentor: Frank Lu

ABSTRACT

The analysis and design of a thin-film gauge (TFG) for implementation in a shock tube installed at the Aerodynamics Research Center is described. The design of the gauge is based on different parameters and constraints that serve to improve the TFG from previously constructed gauges. An analysis of the design was performed to determine the behavior of the gauge with incoming heat flux, simulating the occurrence in the shock tube. Previously constructed TFGs have failed due to the immense pressure that the gauge experiences in the shock tube. For this purpose, a structural analysis was performed to determine the TFG pressure threshold before failure. A numerical analysis of the shock tube flow was performed to obtain a basis for the pressure load on the TFG. The behavior predicted by existing models of the TFG is reflected in the computational analysis performed. Further development of the analysis and design is discussed.

Accurate determination of heat transfer is critical to the design of various aerospace components. Some of these components include the forebody of high-speed vehicles and turbines. The heat load affects the design, such as by imposing a temperature limit to safe operation; the need to use special, high-temperature materials; and the inclusion of cooling strategies. Specifically, for very high-speed vehicles, namely hypersonic vehicles that travel at more than five times the speed of sound, heating rates can be obtained in ground tests using impulse facilities with run times of 0.1–10 ms [1]. One class of impulse facilities used to study the hypersonic heating environment is the shock tunnel. The transient conditions that occur in these facilities require techniques and instrumentation capable of fast response due to the short run time.

When a surface is suddenly heated by the hot gas, its temperature starts to rise. Resistance temperature detectors (RTDs) measure this rapid temperature rise. RTDs for aerospace testing are generally custom-made using platinum, because of its ability to withstand oxidation and ease of manufacture. Commercial RTDs are not suitable due to their long time response. Although platinum is the commonly used material, other metals may also be suitable. As a general requirement, the metal should be capable of being applied as a thin film, which would reduce the response time and also ensure that it is as nonintrusive as possible [2]. The metal should have a high thermal coefficient of resistivity and exhibit linear behavior between resistance and temperature [1]. It should be corrosion-resistant and maintain its solid phase in the temperature range of operation [1]. Examples of metals that meet the requirements described are copper, nickel, tungsten, and platinum.

1.1. Principles of Thin Film Gauges

RTDs used for aerodynamic testing using impulse facilities are also known as thin film gauges (TFG). TFGs are made of an insulating substrate with low thermal conductivity on which a conductive thin film is applied [1]. As mentioned above, the thickness of the TFG is significantly small so as to be nonintrusive and to allow for quick response time of a few microseconds. The TFG is a passive device and is usually built into one arm of a Wheatstone bridge arrangement [3]. The temperature change causes the resistance of the TFG to change. These changes in resistance are small and can be picked up as a voltage change through the Wheatstone bridge arrangement. The output voltage can then be amplified, conditioned, and digitized.

1.2. Objective

The objective is to develop a method to quantify the thickness of the thin film sensor accurately to produce a thin-film heat gauge that has a fast response time and that can withstand the harsh environment of a shock tunnel. The design of the gauge must consider the fabrication process, especially in using conventional methods as far as possible. An analysis of the heat penetration on the TFG will be conducted with the purpose of predicting the surface temperature. In previous TFGs fabricated, the failure factor was the inability to sustain the large pressure load produced by the shock wave in the shock tube. An analysis of the pressure load on the TFG will be conducted to predict the load limit.

Thin Film Gauge

2.1. Principles

The gauge operates on the principle that the resistance of metals increases with a rise in temperature [1]. How fast the temperature rises, for a given material and thickness, depends on the heating rate, also known as the heat flux. Thus, the technique is to measure the surface temperature history in a nonintrusive manner via the TFG. The transduction principle for the TFG is a linear relationship between temperature and resistance.

$$R(T) = [1 + \alpha_R(T - T_o)] \cdot R_o \quad (1)$$

R is the film resistance at surface temperature T, and R_o is the resistance at a reference temperature T_o, and R_o is the film temperature coefficient of resistance of the film [1]. Most metals exhibit the linear behavior so long as the temperature is within the appropriate range.

The basic principles of the TFG for impulse facility applications are illustrated in Figure 1, where the thin film (medium 1) is theoretically infinitely thin such that it does not affect the

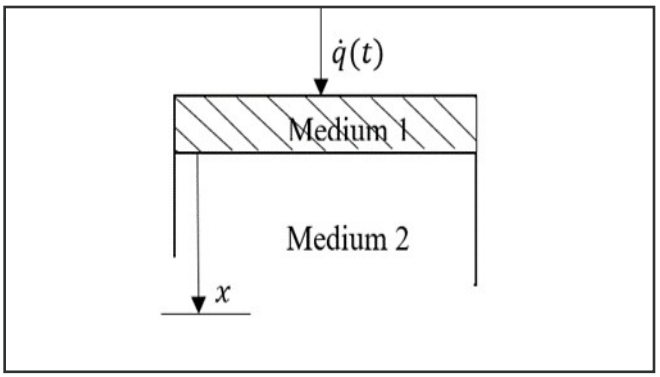

Figure 1. Diagram of TFG Relations

Certain assumptions are made in the design of TFGs according to theory. These are that the heat transfer is one-dimensional, the substrate is semi-infinite and the substrate is a thermal insulator with negligible heat conductivity. The one-dimensional heating essentially ignores heat leakage to the side of the gauge. Heating to the side can be ignored if the gauge is properly insulated or if the heating occurs in a short time. The semi-infinite substrate implies that the far surface is not affected by the heating and remains at ambient conditions. In practice, the substrate should be long enough. Finally, heat at the surface does not flow into an insulating substrate that also supports the semi-infinite requirement.

2.2. Substrate Thickness

The thickness of the substrate is used to validate two of the assumptions that govern the function the gauge. The heat penetration of the substrate should be minimal, similar to that into a semi-infinite solid. The minimum thickness of the substrate that will satisfy the assumptions is obtained by considering the substrate base temperature to surface temperature ratio [1]. Assuming the heat flux isconstant into the substrate surface, the ratio is [1]

$$\frac{T(x,t)}{T(0,t)} = \exp\left(-\frac{x^2}{4\alpha t}\right) - \left(\frac{\pi}{\alpha t}\right)^{1/2}\frac{x}{2}\operatorname{erfc}\left[\frac{x}{2(\alpha t)^{1/2}}\right] \qquad (2)$$

where α is the thermal diffusivity of the material of the substrate and x is the distance the heat penetrates the substrate (see Figure 1).

Since the temperature at the base of the substrate must be a constant temperature, in this case, ambient temperature for all testing time, the ratio of heat penetration is negligible. The ratio is graphed for different time intervals, and the results are displayed in Figure 2. The thermal diffusivity was used for MACOR, a ceramic material that was selected for the substrate. The penetration depth increases gradually as the time interval increases. The time interval in which the shock occurs in the shock tube is approximately 10wms [1], in which the heat penetration in the substrate reaches less than 1 mm. The minimum thickness necessary is then negligible. For structural purposes, the substrate is over 3 mm long, which satisfies the semi-infinite assumption.

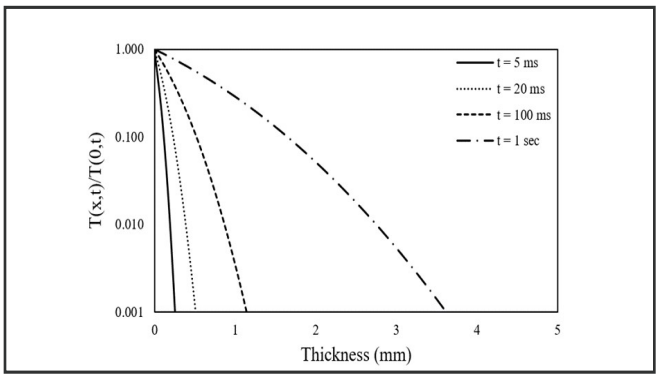

Figure 2. Temperature Depth at Different Time Frames

2.3. Material Selection

The material for the substrate must be insulating to prevent a significant heat penetration depth, satisfying the semi-infinite assumption. The substrate selected was MACOR, a type of machinable glass ceramic, for its thermal properties. The ceramic has a low thermal conductivity and high thermal diffusivity as compared with two commonly used substrate materials. Table 2 compares the thermal properties of four metals. Of the four metals, nickel has the highest thermal conductivity and has the fastest response time, as seen in Figure 3. Although platinum is the most commonly used material, for this study, nickel was selected because of its thermal properties as well as its cost. Nickel, although it has fast response time, has a limited temperature range of operation where linearity between resistance and temperature exist. The TFG will operate in this temperature range.

Material	ρ (kg/m^3)	c $(J/kg \cdot K)$	α $(m^2/s)\ 10^{-9}$	k $(W/m \cdot K)$	$\sqrt{\rho ck}$ $(J/m^2 \cdot K \cdot s^{1/2})$
MACOR	2520	790	733	1.46	0.171
Pyrex	2220	775	756	1.30	0.149
Quartz	2210	755	839	1.40	0.153

Table 1. Thermal Properties of Insulating Material

Material	ρ (kg/m^3)	c $(J/kg \cdot K)$	k $(W/m \cdot K)$	$\sqrt{\rho ck}$ $(J/m^2 \cdot K \cdot s^{1/2})\ 10^3$
Platinum	21400	130	71	14.1
Nickel	8900	440	88	18.6
Tungsten	19600	130	17	20.9
Copper	8940	390	39	37.3

Table 2. Thermal Properties of Conductor

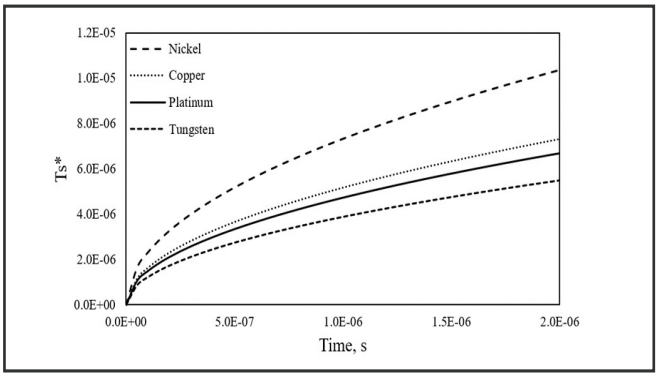

Figure 3. Variation of Surface Temperature and Heat Flux with Time

Shock Tube

The shock tube is composed of a driven and driver section separated by a diaphragm (Figure 4), which breaks at a high pressure difference. The driven section is kept at ambient conditions while the pressure in the driver increases. The initial temperature in the driver and the driven section is at an ambient temperature of approximately 25 degrees Celsius. A one-dimensional, theoretical analysis of the properties of the shock tube and resulting

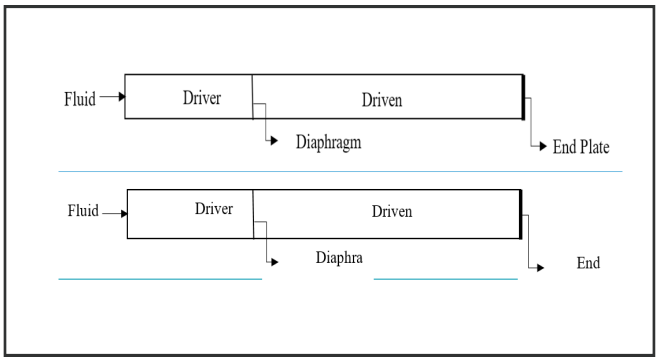

Figure 4. Schematic of the Shock Tube

quantities was conducted to see the flow of the shock.

Once the pressure reaches a desired value or pressure difference limit, the diaphragm will burst sending a shock wave into the driven section and an expansion into the driver section as shown in Figure 5. The shock wave has a front side, region 1, and a backside, region 2; the pressure ratio between region 2 and region 1 is referred to as the shock wave strength or speed. Regions 2 and 3 make the contact surface that has the same velocity and pressure.

The initial conditions are displayed in Table 3, where ideal conditions were assumed. The speed of sound was calculated at ambient conditions in air. The pressure of the driver section is determined based on the diaphragm thickness and scoring depth. In this study, the driver pressure was obtained from a study conducted [3].

$$\frac{p_4}{p_1} = \frac{p_2}{p_1}\left(1 - \frac{(\gamma-1)\frac{a_1}{a_4}\left(\frac{p_2}{p_1}-1\right)}{\sqrt{2\gamma}\sqrt{2\gamma+(\gamma+1)\left(\frac{p_2}{p_1}-1\right)}}\right)^{\frac{-2\gamma}{\gamma-1}} \quad (3)$$

The initial pressure ratio between both sides of the diaphragm is given as p_4/p_1. Using Eq. 3 the pressure ratio of the initial shock wave was calculated. In Excel, Goal Seek, a prediction analysis tool, was used to solve for the shock wave pressure ratio. [4]

The pressure on either side of the contact surface, region 2 and region 3, is the same; p2 = p3. Similar to the relations between the pressures p2 and p3, the velocities across the contact surface are the same. The pressure ratio in Eq. 4 is the strength of the expansion wave. [5]

$$\frac{P_3}{P_4} = \frac{P_2/P_1}{P_4/P_1} \quad (4)$$

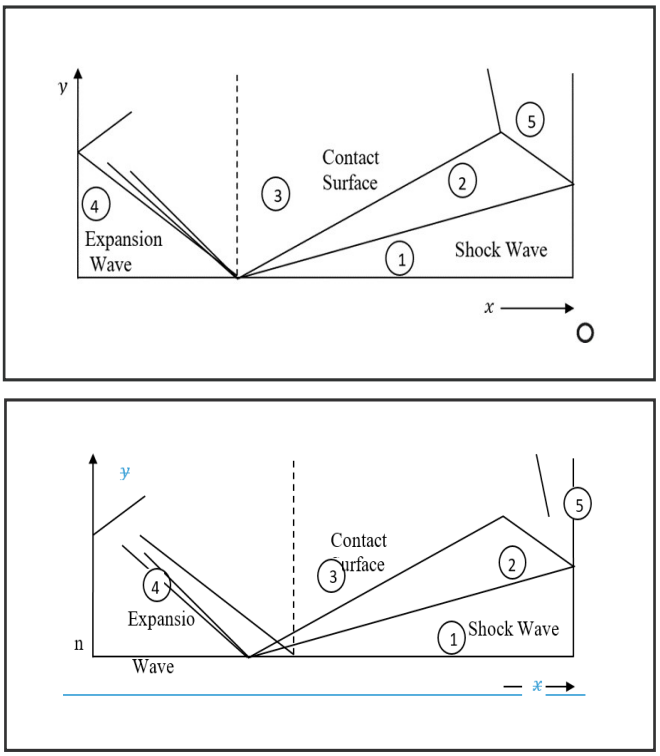

Figure 5. Shock Propagation Diagram

Property	*Value*	*Units*
P_1	101.35	MPa
$T_4 = T_1$	298	K
$V_4 = V_1$	0	m/s
R	287	J/kg·K
g	1.4	-

Table 3. Initial Condition for Shock Tube

Across the contact surface the pressure and velocity are the same, while the temperature and density are different. The expansion and shock waves travel in opposite directions (Figure 5), affecting the temperature differently. The moment the diaphragm bursts, a shock wave is produced traveling into the driven section heating the air flow in region 2, whereas an expansion wave is sent into the driver section cooling the airflow in region 3. Using isentropic relations and assuming ideal gas, the temperature ratio can be obtained. Eq. 5 is used to find the temperature ratio of T3/T4 and the ratio T2/T1 is found using Eq. 6. These equations can be used to solve for the temperature ratio across regions 3 and 2. [6] [7]

$$\frac{T_3}{T_4} = \left(\frac{P_3}{P_4}\right)^{\frac{(\gamma-1)}{\gamma}} \tag{5}$$

$$\frac{T_2}{T_1} = \frac{1+\frac{\gamma-1}{\gamma+1}\frac{P_2}{P_1}}{1+\frac{\gamma-1}{\gamma+1}\frac{P_1}{P_2}} \tag{6}$$

As stated previously, the velocity across the contact surface is the same, which is obtained using Eq. 7. [6]

$$V_{shock} = a_1\left(\frac{P_2}{P_1}-1\right)\sqrt{\frac{2/\gamma}{(\gamma+1)\left(P_2/P_1\right)+(\gamma-1)}} \tag{7}$$

The speed of the shock wave is obtained using Eq. 8 in order to estimate the time it takes the shock to reach the TFG. Using shock speed, the Mach number can be obtained by dividing the shock speed by the speed of sound in region 1. Similarly, the Mach number for regions 2 and 3 can be obtained dividing the velocity by the speed of sound at the corresponding temperature in each region. [5]

$$V_{shock} = a_1\sqrt{\frac{(\gamma+1)}{2\gamma}\left(\frac{P_2}{P_1}-1\right)+1} \tag{8}$$

Using this information, a preliminary approximation of the flow behaviors in the shock tube can be used to analyze the TFG reaction force due to the pressure load it is exposed to.

Results and Discussion

4.1. Design of Thin Film Gauge

A review of previous designs for use in a shock tube underlined necessary constraints and parameters that will improve the sensor's structural and analytical performance. A reduction in complexity allows for ease of manufacturing while reducing cost. This requirement is necessary due to the number of sensors that need to be made; having a simple geometry reduces the time it takes for manufacture. In addition, the TFG must be able to support a large pressure load as produced by the shock wave. While a theoretical analysis of the flow properties within the shock tube was performed,

the properties vary depending on the experiment being conducted. This parameter is important because of the structural failure of TFGs previously manufactured for this purpose. Another important factor is the stability of the sensor in the shock tube flow. It should properly measure the surface temperature of the thin film. To satisfy the one-dimensional assumption, the sensor must be leveled with the surface of the substrate in the direction of the shock wave. Similarly, reliability and accuracy are imperative to the design and functioning of the TFG. The performance of the sensor is essential to ensure results are representative of the flow. The accuracy of the sensor is an important requirement that affects response time. To address this problem, the size reduction of the substrate diameter will increase the accuracy and response time of the sensor.

The TFG will be used as an instrument for experimentation; this means that it will not necessarily hold its original setup. In order to allow for adjustment, a supporting apparatus will be designed (Figure 6). In addition to functionality, the support apparatus will help address the stability and durability of the sensor.

The design will include a protective sheath that encloses the substrate on which the thin film will be placed. The protective sheath is a hollow cylindrical tube made of steel to prevent damage to the substrate. The substrate, a solid cylindrical body, is placed inside the sheath. The thin film will have gold connections that will be drawn on the side of the substrate. Gold is used to connect the thin film to electrical copper wires because gold does not diminish the thermal conductivity of the film and does not disturb the thin film. The electrical copper wire and gold connection will be shielded inside the sheath to prevent damage to the junction. The electrical wires are connected to the gold leads and used to connect to the Wheatstone bridge [1].

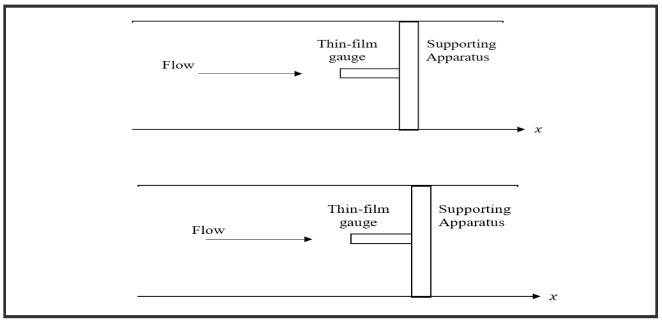

Figure 6. Diagram of TFG Setup

4.2. Analysis Preparation

A mesh is a partition of the model space into elements that are used to approximate equations and solutions. The mesh size of a model can be refined by tools provided by ANSYS, which include refinement tools, method of meshing, and manual input of element size. In order to construct an appropriate mesh for the sensor, a mesh convergence analysis was performed. The purpose for the mesh convergence is to find the optimal mesh size that validates the use of the mesh size, reduces computational time, and produces accurate results. The mesh convergence was performed by looking at the number of elements and solution values. The number of elements that resulted in the mesh converge was 127,080. This was obtained by refining faces on the substrate and thin film surface.

A thermal singularity occurs at a point where the solution does not converge. In this problem, the singularity occurs at the center of the substrate, where the radius of the substrate is zero. The solution at this point approaches infinity due to the lack of convergence. The issue was addressed by changing the meshing method and refinement on the substrate surface. The meshing method chosen was tetrahedron with path conforming at a refinement of 0.0001. This method is used for an adaptive mesh refinement and is good for modeling any kind of geometry. On the substrate surface, the tetrahedron method does not fix a node at the singularity; instead, it works its way around.

4.2.1. Thin Film Gauge. A transient thermal and structural analysis was performed on the developed TFG design to determine the temperature behavior and structural stress experienced due to the pressure load produced by the shock wave.

In the thermal analysis, boundary conditions were imposed on the model to satisfy the one-dimensional semi-infinitew assumptions. The boundary conditions include a perfectly insulated barrier on the outer surface of the protective sheath, a constant temperature on the substrate base of 22 degrees Celsius, and a heat flux on the surfaces normal to the flow. The surrounding temperature is set to an initial value of 22 degrees Celsius. A time step of 11 with an interval of 0.01 ms is set for data collection.

The thermal analysis demonstrated the heat concentration on the thin film as predicted due to

the high thermal conductivity. Although the behavior reflected the operating theory, the values obtained for the surface temperature did not change from the initial temperature. It can be inferred that a mistake occurred in the simulation preparation or boundary condition assignment. The simulation results can be seen in Figure 7.

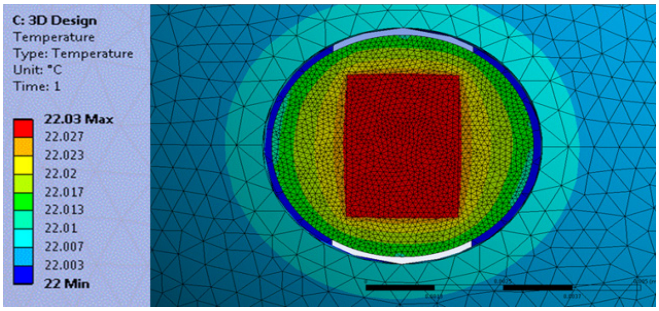

Figure 7. Top View of TFG in Thermal Analysis

Similarly, in the structural analysis, obstacles became apparent when adding the boundary conditions. The analysis was simplified by looking at the axial forces and neglecting forces in other directions. The analysis was conducted using the calculated value for the pressure load on the sensor. This pressure load is dependent on the experimental proceedings set in which the TFG will be used in.

4.2.2 Substrate Analysis. A transient thermal analysis was performed to determine the temperature history over time at an applied heat flux in the substrate. The boundary and initial conditions are the same as those described for the gauge. The results obtained for the substrate do reflect the theory and the heat penetration depth, as seen in Figure 8. Although, the simulation results seem to follow the predicted trend, the result values are not accurate.

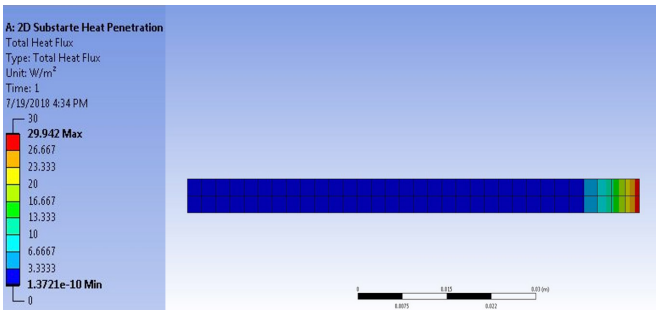

Figure 8. Two-dimensional Thermal Analysis of Substrate

Conclusion

The results obtained from the thermal analysis suggest that something went wrong while setting up the simulations. The objective of this study was to develop a design and conduct analysis to see how the predicted behaviors occurred. A number of constraints and parameters were set on the design. The requirements served to underline the important characteristics of the TFG and how it would be addressed in the design. The transient thermal analysis of the TFG and substrate reflected the theoretical behavior of the heat penetration but the resulting values did not.

Acknowledgments

I would like to thank my parents for supporting my ambitions, for without their emotional and financial support, I would not have the opportunity to expand my knowledge and skills through an enriching experience. I would like to thank the McNair Scholars program, for the opportunity to participate in research this summer. My advisor, Dr. Frank Lu, was a friendly and supportive mentor while embarking on this invaluable experience. Dr. Frank Lu is a laudable professor at UTA, whom I hold in high regard for his dedication to his students. I would like to thank Umang Dighe, a graduate student working under Dr. Frank Lu, for the time he dedicated to offer advice on different areas of my research.

Nomenclature

x	axial length
M	Mach number
P	pressure
R	resistance
a	speed of sound
T	temperature
k	thermal conductivity
t	time
v	velocity
ρ	density
γ	specific heat
α	thermal diffusivity

Subscripts

o	Ambient condition
s	Surface

References

K. Kinnear, "Design, calibration and testing of transient thin film heat transfer gauges," Masters thesis, The University of Texas at Arlington, Arlington, TX, Dec. 1997.

T. E. Diller, "Advances in heat flux measurements," Advances in Heat Transfer, vol. 23, pp. 279-368, 1993.

D. G. Leamon, "Characterization of hypersonic shock tunnel," Masters thesis, The University of Texas at Arlington, Arlington, TX, May 2012.

C. M. Seitel, "Comparing the inviscid and viscous flows in a shock tube to analyze the boundary layer effects," Masters thesis, The State University of New Jersey, New Brunswick, New Jersey, Jan. 2009.

H. W. Liepmann and A. Roshko, Elements of Gas Dynamics. Mineola, NY: Dover, Jan. 2002.

N. Martins, M. G. Carvalho, N. H. Afgan, and A. I. Leontiev, "Design and sensitivity analysis of a new gauge for radiation heat flux assessment," Heat and Technology, vol. 16, no. 2, 1998.

J. D. Anderson, Fundamentals of Aerodynamics, 6th ed. New York, NY: McGraw-Hill, 2017.

McNair Scholars Research Journal
Vol. 22 • 2018
ISSN 2642-2492
doi:10.32855/mcnairscholarsuta.2018.004

PRESSURE ULCER PREVENTION USING SOFT, NON-GRASP MANIPULATION

REGAN KUBICEK
DEPARTMENT OF MECHANICAL AND AEROSPACE ENGINEERING

Faculty Mentor: Alan Bowling

ABSTRACT

"Hard and soft" body manipulation have long been studies applied within the field of biomedical engineering. Further research within this field has the capability of revealing many hidden secrets of how the human body changes when in contact with various surfaces. The object in this study is the human body, and the goal is to manipulate the size and duration of contact forces acting on the skin to prevent the formation of pressure ulcers (PUs). In doing so, the primary product of this experiment is to create a "Forcebed" capable of shaping itself to the human form in order to collect a time history of pressure distribution across the subject's body. Through data collection of contact forces on the patient's skin, the Forcebed can autonomously offload high concentrations of normal and shear forces by means of redistribution. This method of redistributing forces prevents any form of direct grasping on the patient's body. We refer to this method of object control as soft, non-grasp manipulation. This is accomplished through a soft flexible human-robot interface in tandem with a parallel closed chain rigid mechanism. The device presented in this work is a novel approach to the detection and prevention of PUs.

1.1 Motivation

A pressure ulcer (PU), also known as a bed sore, is localized damage to the skin which usually occurs over a bony prominence of the body. Pressure ulcers develop due to intense and/or prolonged exposure of pressure and shearing forces on the skin [1]. Hospital patients with long durations of bedrest and elderly persons in nursing homes have the highest risk of developing PUs. Frequent sites of PU occurrence include the skin covering the coccyx, sacrum, heels, and hips. Figure 1.1 illustrates different stages of pressure ulcer formation.

Figure 1.1. Pressure Ulcer Stages

Pressure ulcers are one of the most common health conditions in the United States affecting approximately 2.5 million individuals annually at a treatment cost of between $9.1 and $11.6 billion every year [2]. An estimated 60,000 Americans die each year as a direct result of complications associated with pressure ulcers [3]. Prevention and clinical treatment guidelines are outlined by the National Pressure Ulcer Advisory Panel (NPUAP). Under the current revision [4], "care-givers should strive to reposition an individual receiving palliative care at least every 4 hours on a pressure redistributing mattress such as viscoelastic foam, or every two hours on a regular mattress." This method of physically rotating the person can be problematic as there is risk to both the patient and the nurses implementing the protocol. When rotating the patient manually, additional shear strains can be induced, thus exacerbating PU formation. Additionally, back injuries to staff are a major concern when lifting heavy patients. The frequency of every two to four hours puts additional strain on the nursing workforce along with the possibility of compromising patient health. Due to this rigorous regime, the standard operating procedure for PU prevention may not be implemented in its entirety. In a nationwide study in 2011 [5], "only 10.8% of the patients at risk received fully adequate prevention in bed and while sitting."

This paper presents a novel approach to PU monitoring and prevention through the development of a robotic bed.

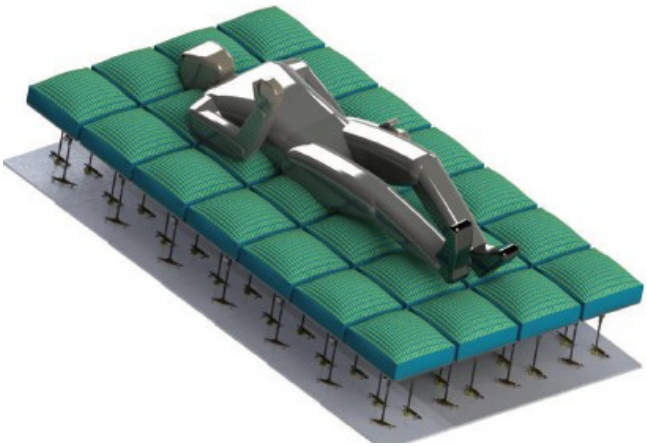

Figure 1.2. Forcebed.

The device proposed is the "Forcebed" illustrated in Fig 1.2. As previously discussed, the current prevention technique is a two to four hour rotation schedule to relieve contact forces concentrated on the body. There are numerous devices currently in use that attempt to prevent the formation of PUs [6]. Unlike current devices, which still require the care-giver to turn the patient, the Forcebed will provide complete autonomy of PU prevention. The Forcebed will allow shear and pressure forces to be offloaded and redistributed in a way that minimizes the magnitude and duration of forces on the patient. This is accomplished with little to no patient movement and no assistance from the care-giver. To understand and monitor the formation of PUs, it is necessary to document the history of pressure distribution across the patient. The Forcebed will utilize a multi-modal sensor grid that provides a time history of force feedback for the model-based force control [7]. The sensor grid will provide a

large number of measurements over the patient's skin to investigate the underlying causes of PU formation.

1.2 Design Hypothesis

The primary goal of the Forcebed is to provide soft, non-grasp manipulation that allows contact forces acting on the body to be distributed such that there is no firm grasp on any part of the patient. Fig. 1.3 illustrates four different bed configurations and examines the resulting forces for each. Fig. 1.3a depicts a mattress that is highly pressurized.

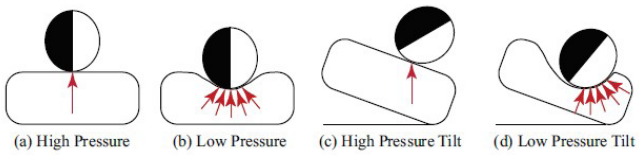

Figure 1.3. Contact forces for various configurations.

This configuration directs a large normal force on one specific area. By decreasing the pressure in the mattress, the force is distributed across a larger area (Fig. 1.3b). Decreasing pressure minimizes high concentration forces, but provides no means of offloading these forces. Fig. 1.3c shows adding a tilt to a stiff surface. This creates large normal and shear forces on the skin that are concentrated in a specific area. Fig. 1.3d illustrates what is referred to as a soft, non-grasp manipulation. The forces are distributed resulting in lower normal forces. Shear strain on the skin is also minimized, and the tilt feature allows for forces to be offloaded. Achieving this soft, non-grasp manipulation is important in reducing the magnitude of normal and shear forces acting on the patient, and therefore is imperative to PU prevention.

Several criteria must be considered when designing a device to achieve this non-grasp manipulation. An end-effector is defined simply as the robot-object interface. When the object to be manipulated is the human body, it is important to construct the end-effector with a material that closely resembles soft biological materials. Conventional materials used in robotics, such as metal, generally have an elastic modulus in the order 10^9-10^{12} pascals. Whereas natural organisms, such as muscle tissue and skin, fall within a range of moduli between 10^4-10^9 [8]. The end-effector must also provide a dynamic range of stiffness. A large variation of stiffness ensures the human body can be supported while also keeping contact forces on the patient to a minimum. The manipulator must be capable of a wide range of articulation to ensure contact forces can be offloaded from the body. The manipulator must also rotate the patient as necessary without the use of a care-giver.

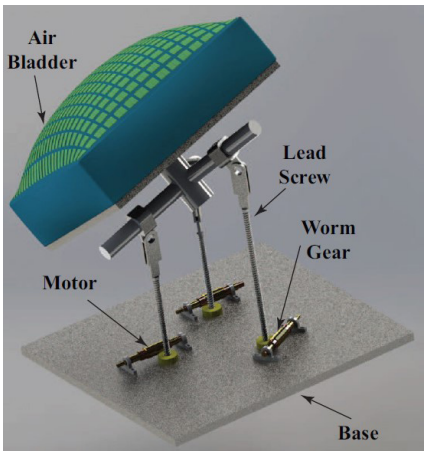

Figure 1.4. Forcebed tile illustration.

This criterion led to the development of a hybrid hard and soft manipulator, referred to as the "Forcebed Tile," illustrated in Fig 1.4. The air bladder will be made from silicone rubber with an elastic modulus of $10^{7.}$ meeting the material capability to handle the human body safely. The air bladder also demonstrates the ability to inflate and deflate giving the patient support while still minimizing the magnitude of contact forces. The bladder is used in tandem with a parallel closed chain mechanism which provides sufficient dynamic range to either rotate the patient or assist in offloading contact forces. A sensor grid attached to the top of the bladder will provide shear and normal force feedback. This multi-modal sensor is still in development [7], a preliminary model will be presented in this paper. The Forcebed Tile is just one of 28 tiles that work in unison to create the Forcebed (Fig. 1.2). The Forcebed will provide

a time history of patient position and force feedback permitting the redistribution of contact forces on the patient's skin by means of soft, non-grasp manipulation.

1.3 Model-Based Force Control

Robots constructed from soft materials and driven by fluids cannot yet be modeled or controlled accurately. This is largely due to the complex and dynamic movement that these soft robots can achieve [8]. For this reason, object manipulation and grasp control, be it for rigid or flexible objects, still proves to be a challenging issue. The major challenge in using soft manipulators is accurate object position control. Due to the range of deformation and morphology that can occur in soft robots, traditional means of feedback such as encoders or inertial measurement units (IMUs) cannot be used [8]. Soft robots made from elastic materials require flexible or stretchable sensors for the functional feedback necessary in closed-loop control [9]. There is an abundance of research currently in the field of stretchable electronics [10], which is too extensive to cover in this work. However, the current use of stretchable sensors for use in soft robotic manipulators is limited. Thus, flexible robots lack 'sense' due to the absence of haptic feedback during object manipulation. Vision sensing can be used in some cases to allow for object position detection. However, vision is not an acceptable source of feedback for our application because it cannot determine contact forces on the skin. Furthermore, our design is not focused solely on position control but rather a hybrid position/force control. A preliminary force sensor for this application is in current development in our lab (Section 2.2). In the process of offloading contact forces, the position of the patient may or may not change depending on the force distribution. Forces can be offloaded from an area of the patient without repositioning the individual, making this hybrid position/force control a desirable approach. It is through this method that soft, non-grasp manipulation is possible. To achieve soft, non-grasp manipulation of an object a closed-loop model-based hybrid operational space position/force control is proposed.

Design

2.1 Mechanical

The mechanical design began in 2011 as a team effort. The mechanism consists of a parallel closed chain mechanism as observed in Fig. 2.1 and can be compared to the labeled illustration in Fig. 1.4. The worm gear set is powered by brushed DC motors. The three worm gears rest on thrust bearings and each one actuates a respective lead screw. On top of each lead screw are swivel ball joint rod ends. Each ball joint allows for 65° of travel, which is also the max articulation of the top plate with respect to the horizontal plane. The air bladder is made from high strength silicone rubber and fastened directly to the top plate. Inflation of the bladder is made possible through an external air compressor.

Figure 2.1. Forcebed tile prototype.

2.2 Electronics Package

The electronics package started as my individual project in 2017. Each element of the Forcebed Tile electronics can be observed in Fig. 2.2. The package consists of tw o micro-controllers, three incremental optical encoders, three brushed DC motors, three motor drivers, three limit switches, two multiplexers, a triple-axis gyro, a pressure transducer, and the force sensor matrix (Fig. 2.3). The three brushed DC motors control each worm gear set independently of one another. Incremental shaft encoders are used to provide position feedback of the motors to the primary

controller. An Arduino Mega is used as the primary controller and an Arduino Uno as the secondary. The Arduino Uno monitors the function of the pressure sensor matrix by way of the two multiplexers. The Mega receives force sensor data from the Uno and the motor encoders, while also acting as the motor controller. The limit switches provide a "home position" for each Forcebed Tile; this is used during initial power-up such that the tile can establish its initial position in the operational space.

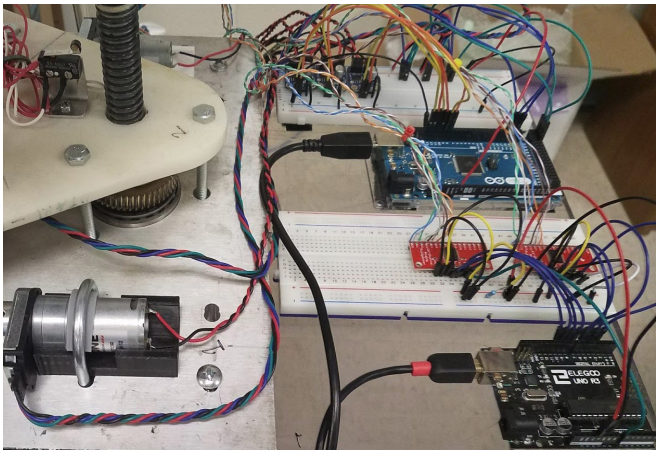

Figure 2.2. Electronics package.

2.3 Force Sensor Matrix

Development of a preliminary force sensor was necessary to ensure the computer model of the bladder matches the physical bladder (Section 4.1). The final sensor package that will incorporate shear and pressure sensors is still in development [7]. A picture of the force sensor matrix is found in Fig. 2.3. The matrix is made from a woven mesh of stainless steel thread. Each intersection of woven thread represents one sensor. The fabric that the stainless-steel thread is woven through is a piezo-resistive cloth. When force is applied to the cloth, the resistance measured between the top and the bottom of the cloth decreases. A voltage differential is applied across the two intersecting wires completing the circuit. As force is applied at each intersection, the resistance in the cloth changes creating a measurable change in the voltage. This change in voltage is monitored via the analog input from the Arduino

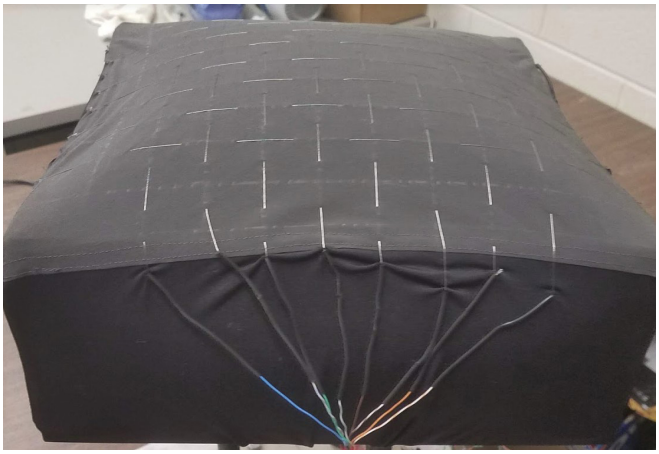

Figure 2.3. Force sensor matrix.

The two multiplexers combine to provide a unique binary address set for each sensor. The Uno is connected to two multiplexers. The two multiplexers combine to provide a unique binary address set for each sensor. The existing sensor capabilities with two 16 channel multiplexers is 256 sensors; however, a higher resolution matrix consisting of 1,024 sensors is planned (Section 4.2).

Model

3.1 Rigid Body Model

The rigid body model is composed of the parallel closed chain mechanism. Fig. 3.1 illustrates the frame and coordinate assignments for the mechanism. Point N signifies the inertial reference point, and the inertial reference frame is represented by N1, N2, and N3. The kinematics of the rigid body mechanism can be completely defined with 9 generalized coordinates. A1, B1, and C1 represent the height of each lead screw with respect to the bottom plate. Lengths a, b, and c signify the distance from the ball joint rod ends to point P. Lastly, q1, q2, and q3 denote the orientation of the top plate. The mechanism has 3 degrees of freedom (DOFs) and 9 generalized coordinates. Due to having more generalized coordinates than DOFs, some coordinates must be measured directly. Coordinates A1, B1, and C1 can be determined by the relationship

formed with the encoders. Every rotation of the motor correlates to a height change in the respective lead screw. By measuring the motor position with the incremental encoders, these coordinates can be found. A three-axis gyro is used to measure the orientation of the top plate directly. This satisfies 6 of the generalized coordinates. With 3 coordinates remaining and 3 DOFs, the system can be solved for.

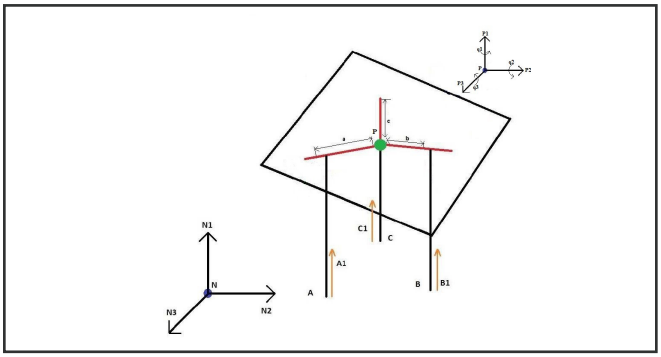

Figure 3.1. Generalized coordinates and frames.

3.2 Soft Body Model

This approach to modeling the air bladder has been largely adapted from previous work in our lab [13]. The simplest form of simulating a flexible system is by discretizing the material into a spring mass damper (SMD) system. The mass in the system will be represented as a massive particle. A massive particle is an infinitesimally small body that has mass to it. Because a particle is infinitesimally small, no reference frame is attached. This simplifies the system by not taking an interest in the body's rotation. A simple example of a spring mass damper system can be observed in Fig. 3.2. The spring force F_k is given by:

$$F_d = -k(x - L_0) \cdot \hat{N}1 \tag{3.1}$$

Where $\hat{N}$ k is the spring constant, Lo is the unstretched length of the spring and x is the spring length after stretching or compressing. Damping force F_d is given by:

$$F_d = -c\dot{x} \cdot \hat{N}1 \tag{3.2}$$

c is the damping coefficient and $\dot{x}$ represents the linear velocity of the mass. The acceleration a of the particle is given by summing the spring and damping forces:

$$a = M^{-1}(F_k + F_d) \tag{3.3}$$

By integrating Eqn. 3.3, the velocities and position of the particle can be found.

By linking several spring mass damper particle systems together, a spring mass damper chain can be formed (Fig 3.3). We can apply the spring mass damper chain technique to an N number of rows and columns to achieve an SMD matrix (Fig 3.4).

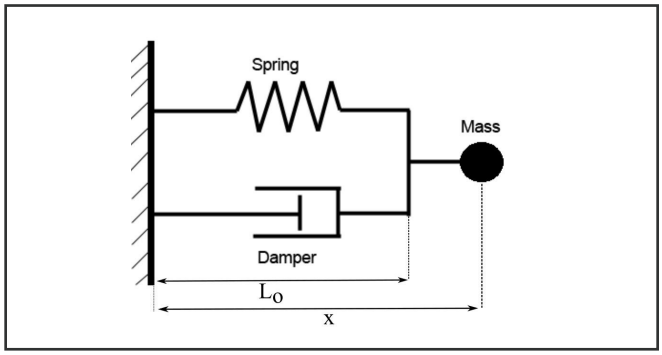

Figure 3.2. Simple spring mass damper.

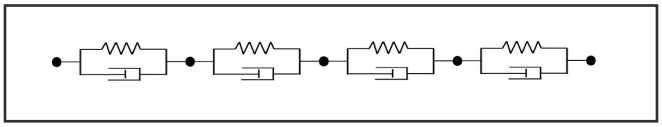

Figure 3.3. Spring mass damper chain.

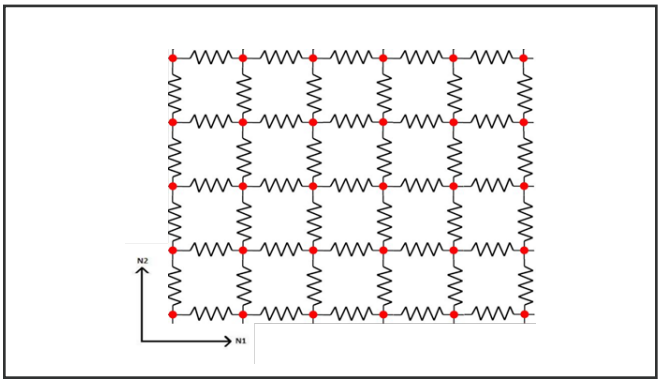

Figure 3.4. Spring mass damper chain.

Thus far we have considered the forces from the spring and damper acting on the particles; however, the force from the internal pressure of the bladder must be incorporated into the model. The force from pressure acting on each particle is given as:

$$a = M^{-1}(F_k + F_d) \quad (3.4)$$

P is the gage pressure inside the bladder, A is the total surface area of the spring mass damper matrix, N is the number of particles in the matrix, and P_C is the direction vector of the applied force due to pressure. Because a particle was chosen, there is no body attached frame to reference the direction vector; therefore, it must be calculated.

Consider Fig. 3.5 illustrating particle P with its adjoining particles A, B, C, and D. By taking the sum of the cross products of the position vectors P_{PA}, P_{PB}, P_{PC}, P_{PD} the direction vector of the force from air pressure acting on each particle can be found (Eqn. 3.5).

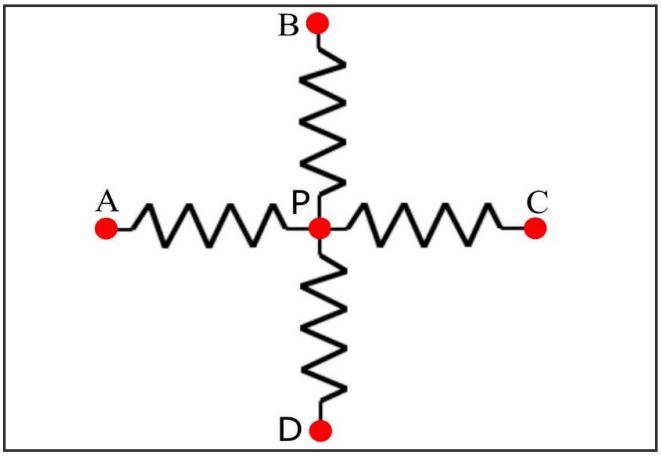

Figure 3.5. Adjacent particles

$$P_C = P[(P_{PA} \times P_{PD}) + (P_{PD} \times P_{PC}) + (P_{PC} \times P_{PB}) + (P_{PB} \times P_{PA})] \quad (3.5)$$

The mass of each particle was determined by dividing the mass of the silicone rubber material used for the bladder with the surface area of the subsequent SMD matrix and dividing by N number of particles in the matrix. With the inclusion of the gravitational force, all forces acting on each particle can now be summed. We are only concerned with describing the translation of each massive particle. This can be achieved by using Newtons Second Law to solve for the acceleration of each particle:

$$a = M^{-1}(F_k + F_d + F_p + F_g) \quad (3.6)$$

MatLab was used to generate a force matrix of the system. Because the system was simplified by choosing particles, there are no inertias in the system; therefore, the mass matrix is simply the corresponding mass of each particle. By solving Eqn. 3.7 in MatLab using an ODE solver the velocities and position of each particle in the SMD matrix can be found. The result is a linear spring mass damper model of the air bladder. The natural progression of inflation can be observed in Figs. 3.6, 3.7, and 3.8.

$$\int \begin{bmatrix} a_1 \\ a_2 \\ a_3 \\ a_4 \\ a_5 \end{bmatrix} = M_{-1} \int \begin{bmatrix} F_1 \\ F_2 \\ F_3 \\ F_4 \\ F_5 \end{bmatrix} \quad (3.7)$$

The values used for the spring constant and damping coefficient were approximated to match the physical bladder through measurements with a digital caliper. A more extensive method for measuring the air bladder and calculating the spring constant is proposed for future work and discussed in detail in the following section.

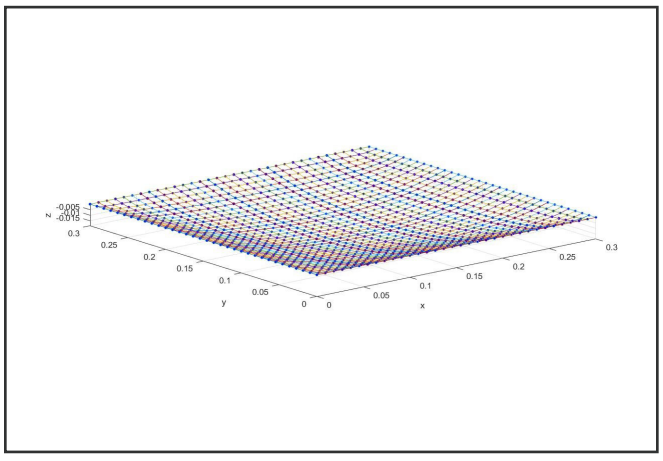

Figure 3.6. SMD Model with 0.00 PSI.

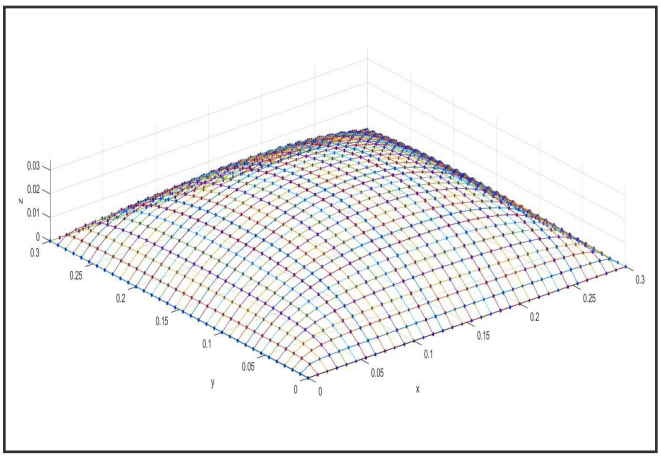

Figure 3.7. SMD Model with 0.05 PSI.

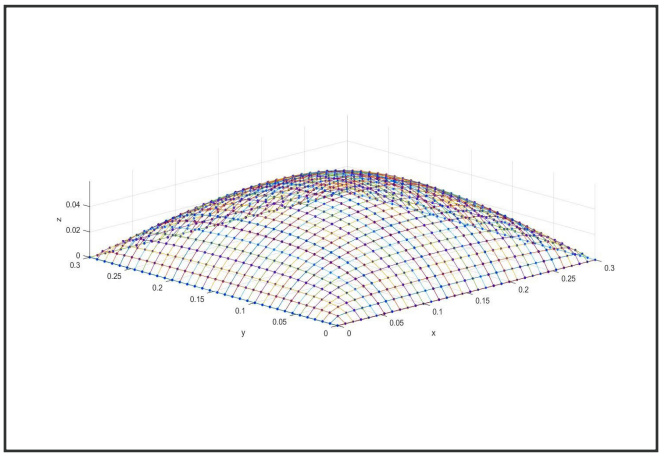

Figure 3.8. SMD Model with 0.30 PSI.

Future Work and Conclusion

4.1 Matching the Model

One of the greatest challenges faced in the model-based design of soft robotics is matching the model directly to the physical object. The bladder, although made from the same material throughout, is not completely homogeneous. It is unlikely that complete uniformity is maintained throughout the material during the manufacturing process. Material properties and thicknesses may vary from one location to another and defects, such as small air pockets, may exist within the material. Perhaps the most obvious reason that a linear spring model cannot match the silicone bladder is that the silicone rubber material exhibits non-linearity. As the material is stretched, the force required to stretch it further must increase. This creates a challenge for matching the SMD matrix model to the actual bladder. A commonly used method of modeling deformable surfaces is the finite element method (FEM). FEM modeling takes the material's property into consideration and is commonly referred to as a strain-stress (stiffness) model [11]. Aside from being computationally expensive for use in control, the FEM model is based on material properties and still must match the heterogenous object.

Due to the aforementioned manufacturing limitations, the end product could have a multitude of variations introducing error into the model. The proposed solution is a non-linear data-driven model. Going back to the SMD model, the spring constant of each spring must be different from every other spring to match the heterogeneity of the physical system. To accomplish this, a grid representing the sensor placement is applied to the top surface of the bladder. Using a coordinate measuring machine (CMM) the cartesian coordinates of each sensor location can be found with respect to an inertial reference point. A data set is then recorded that correlates to a specific internal pressure in the air bladder. By measuring several sets of data at various pressures, a nonlinear regression can be performed to determine the spring constant. This will result in a polynomial spring constant for all 1,156 springs and provide an accurate representation of the bladder. With the model matching the air bladder, position and force data from the force sensor matrix can be fed into the model and real-time deformations can be analyzed.

4.2 Force Sensor Upgrade

The current force sensor (Fig 2.3) has a resolution of 2.5 cm. This is not a dense enough resolution to accurately monitor the position of an object; a higher resolution matrix will be required. Another problem with the current sensor design is that the stainless-steel mesh is not stretchable, inhibiting the accuracy of the model. Several challenges need to

be overcome to create a higher resolution stretchable sensor. We are exploring a variety of options ranging from stretchable inks to stretchable silver thread. The final proposed sensor grid to measure shear and normal forces is still in development [7].

4.3 Conclusion

This paper proposes a novel medical device to aid in the prevention of PUs. The Forcebed will act as a robotic assistant, relieving some of the physical and mental burdens of PU prevention. The Forcebed, which is still in the prototyping phase, will utilize a soft, non-grasp technique towards the prevention of PUs. Through the use of a pressure sensor grid, a time history of force distribution can be acquired, providing further insight into the formation of PUs. With the continuation of this body of research, our goal is to improve patient health and quality of life through the detection and prevention of PUs.

References

[1] Npuap.org, National Pressure Ulcer Advisory Panel (NPUAP) Announces a Change in Terminology from Pressure Ulcer to Pressure Injury and Updates the Stages of Pressure Injury | The National Pressure Ulcer Advisory Panel - NPUAP. Available at: http://www.npuap.org/national-pressure-ulcer-advisory-panel-npuap-announces-a-change-in-terminology-from-pressure-ulcer-to-pressure-injury-and-updates-the-stages-of-pressure-injury/ [Accessed 6 Jul. 2018].

[2] Karen Bauer, Kathryn Rock, Munier Nazzal, Olivia Jones, and Weikai Qu, "Pressure ulcers in the United States inpatient population from 2008 to 2012: Results of a retrospective nationwide study," Ostomy Wound Management, vol. 62, no. 11, pp. 30–38, Nov. 2016.

[3] M. Reddy, S. S. Gill, and P. A. Rochon, "Preventing pressure ulcers: A systematic review," Jama, vol. 296, no. 8, p. 974, Aug. 2006.

[4] Audrey Nelson, John D. Lloyd, Nancy Menzel, and Clifford Gross, "Preventing nursing back injuries: Redesigning patient handling tasks," AAOHN Journal, vol. 51, no. 3, pp.126-134. Mar. 2003.

[5] K. Vanderwee, T. Defloor, D. Beeckman, L. Demarre, S. Verhaeghe, T. V. Durme, and M. Gobert, "Assessing the adequacy of pressure ulcer prevention in hospitals: A nationwide prevalence survey," BMJ Quality & Safety, vol. 20, no. 3, pp. 260–267, May 2011.

[6] McInnes, Elizabeth, et al. "Support surfaces for pressure ulcer prevention," Cochrane Dwatabase of Systematic Reviews, vol 9, pp. 1-119. Sep. 2015.

[7] R. Yousefi, S. Ostadabbas, M. Faezipour, M. Nourani, V. Ng, L. Tamil, A. Bowling, D. Behan, and M. Pompeo, "A smart bed platform for monitoring & ulcer prevention," 4th International Conference on Biomedical Engineering and Informatics (BMEI), Oct. 2011.

[8] D. Rus and M. T. Tolley, "Design, fabrication and control of soft robots," Nature, vol. 521, no. 7553, pp. 467–475, May 2015.

[9] Robert J. Webster III and Bryan A. Jones, "Design and kinematic modeling of constant curvature continuum robots: A review," The International Journal of Robotics Research, vol. 29, no. 13, pp. 1661-1683, Nov. 2010.

[10] N. Lu and D.-H. Kim, "Flexible and stretchable electronics paving the way for soft robotics," Soft Robotics, vol. 1, no. 1, pp. 53–62, Mar. 2014.

[11] Di Cao, "Physically based simulation of various fabrics with multi-level modeling," Ph.D. dissertation, The Ohio State University, 2017.

[12] Photograph by Sadegh Babagolzadeh, distributed under a CC BY-SA 3.0 license. https://commons.wikipedia.org/wiki/File:Wound_stage.jpg. [Accessed July 15, 2018].

[13] Parikh, Pranav. Smart Bed and Contact Impact of Flexible Bodies Using Energy Compensation Method. Diss. 2015.

Volume 22 • 2018

McNair Abstracts

ISSN 2642-2492

McNair Scholars Program

Summer Research • 2018

ABSTRACTS

Matrix-Based Methods of Data Collection and Analysis of Soccer Matches

Henry Alvarez, Mathematics Major

Mentor: Dan Warren, Ph.D.

This paper explores the efficiency of collecting data from soccer games in matrices that will then allow for mathematical or statistical analysis. While these matrices are useful for analysis, they are best used alongside other current statistical, mathematical, tactical, or scientific analysis methods in soccer. Through these matrices, much information can be obtained, such as individual passing percentages and passing frequencies from one player to another. Additional, non-mathematical and non-statistical information that can be derived from these matrices are passing patterns for individual players, such as which teammates a player might receive the ball from the most and who that same player then passes the ball to the most. The most rigorous mathematical application explored is the application of Markov chain steady states. Through some preparations of the matrices, we were able to create Markov chain stochastic matrices. Through these, we found the steady states of the teams' distributions, for example, who received or passed the ball the most in a team, which allowed us to discover biases among the players.

Bassoon: Clown of the Orchestra or Versatile Unsung Voice

Jazmyn Barajas-Trujillo, Music Major

Mentor: Graham Hunt, Ph.D.

Woodwind instruments gained technical advances that increased their versatility following the Baroque period. These advances provided composers with greater opportunity to write more complex parts for winds, which in turn led woodwinds to function as more prominent voices in an orchestral setting. Their growing importance also allowed composers to take advantage of their unique timbral features to depict specific characteristics and topics. Composers, who additionally wrote orchestrational treaties, deduced associations by referencing examples found from within the Classical and Romantic repertoire, and thus created distinct stereotypes for each woodwind instrument, such as the bassoon being associated with the grotesque and clumsy because of its tone color. Focusing on the opera genre, this essay explores how the bassoon, as well as other woodwind instruments can enhance the portrayal of the characters' internal psyche and plot through topical associations. The purpose of this essay is to create a more multidimensional and meaningful understanding of Mozart's operas by creating a motivic network through topical associations in the woodwind section. These topical associations will give the audience member a better insight into Mozart's intricate and allusive use of woodwinds and their contribution to Mozart's operatic masterpieces.

Magnetic and Hyperthermia Properties of $CoFe_2O_4$ Nanoparticles

Julian Beatty, Physics Major

Mentor: Jeotikanta Mohapatra, Ph.D.

The heating properties of magnetic nanoparticles are steadily becoming more relevant because of their applications in the biomedical field: drug delivery, magnetic resonance imaging and, particularly, cancer treatment. Magnetic fluid hyperthermia is an alternative to chemotherapy; it involves injecting magnetic nanoparticles into the cancerous tissue and applying an external alternating magnetic field, causing the nanoparticles to generate just enough heat to halt the growth of cancer without damaging the surrounding healthy tissue. While the treatment shows great promise, the major hurdle is that most commercially available magnetic nanoparticles have low heating rates or toxicity problems, which make them unsuitable for this treatment. The former case is a serious problem because it would require a substantially higher amount of the nanoparticles to be injected into the body, resulting in harmful side effects. This report seeks to address this concern by providing a detailed protocol for synthesizing highly magnetic 12nm $CoFe_2O_4$ nanoparticles with uniform distribution and by demonstrating control over their heating and magnetic properties. Our approach will be to synthesize highly magnetic $CoFe_2O_4$ nanoparticles by fine-tuning their shape, size and composition, which will have the effect of boosting their heating efficiency.

The Relationship between Biopsychosocial Constructs and Functional Health in Older Adults with Chronic Lower Back Pain

Enriqueta Calderon, Psychology Major

Mentor: Robert Gatchel, Ph.D.

Many older adults are confronted with chronic pain. Biopsychosocial aspects need to be considered for older individuals to enhance quality of life. Older adults with chronic lower back pain (CLBP) experience physical and psychosocial obstacles that negatively impact overall well-being. In recent research, exercise interventions have been conducted to show that older adults can improve physically, which assists in reducing pain, fear, and risk of serious health issues. The present study developed an exercise protocol for older individuals with CLBP to assist their physical functioning, balance efficacy, and psychosocial status. Two hypotheses were tested: (1) psychosocial and physical measures would improve with exercise from pre-test to post-test; and (2) pre-test and post-test psychosocial and physical measures would be related to physical functioning scores. These measurements were evaluated through statistical analyses to determine the relationships among the variables. Results revealed that there was statistical significance to partially support the first hypothesis of improvement on visual balance, leg strength, and depression measures. The second hypothesis was also partially supported: fatigue, pain inference, and shoulder flexibility were related to perceived physical function. Overall, though, the results demonstrated support for the use of exercise interventions in enhancing biopsychosocial measures of older adults who suffer from CLBP.

Code Obfuscation Study Using Obfuscator-LLVM

Silvia Chapa, Computer Science & Engineering Major

Mentor: Jiang Ming, Ph.D.

To impede the reverse-engineering of source code, the programmer may choose to use obfuscation techniques for compiling; Obfuscator-LLVM is one software for such purposes. This research collected data on the results of obfuscation with Obfuscator-LLVM, comparing the ordinary compiler's assembly code to that of fifteen combinations of Obfuscator's three primary obfuscations: Flattening, Substituting, and Bogus Control Flows. The resulting binary files were converted to assembly code by using "objdump –d,", and their lines and sections counted. The control flows of the obfuscations were compared with that of the regular compiler version, and base blocks, branch points, merge points, and final base blocks were counted for each function in the non-GUI "Hello World" program that was used as a sample. Assembly code lines and sections were also counted for a more complicated program implementing a "Graham's Scan" algorithm, though for this control flow analysis was limited by size of the resulting files. It was found that the shape of the control flow diagrams was affected differently by the different obfuscations, that there was little change in the number of branch points, merge points, and final base blocks, and that obfuscation resulted in an increase of both assembly code lines and sections.

Effects of FtsQ Phosphorylation on Mycobacterium Septation

Dominic French, Biology and Microbiology Major

Mentor: Cara Boutte, Ph.D.

The extensive treatment time of tuberculosis is in no small part due to the tolerance of antibiotics by Mycobacterium tuberculosis (Mtb) in certain conditions during which Mtb has different physiological characteristics than when it is in exponential growth phase. Using the Mycobacterium model organism Mycobacterium smegmatis, we investigated one of the possible regulation mechanisms involved in modulating antibiotic tolerance. We investigated FtsQ, a cell division regulation protein that is essential to the survival of Mycobacterium smegmatis. It is an integral part of the FtsQLB protein complex. The FtsQLB complex is a core part of the divisome, a series of proteins responsible for regulating the division of the cell. We hypothesize that FtsQ is regulated via phosphorylation and that through this regulation the cell can respond to different environmental stresses. To address this question, phosphoablative and phosphomimetic mutants of FtsQ were constructed in order to test for physiological differences. Our current results suggest that a difference might exist between the strains in the presence of meropenem. Further research is needed in order to confirm the existence of this difference.

Synthesis of 4-Methoxystyrene Derivatives from 4-Allylanisole and Diverse Nucleophiles

Octavio Miranda, Chemistry Major

Mentor: Alejandro Bugarin, Ph.D.

The research presented explores a one-pot synthesis of 4-methoxystyrene derivatives from 4-allylanisole. The reaction is completed in two steps in which 4-allylanisole is first brominated, and then undergoes an elimination and substitution to create the expected final product. When brominated, the starting material is believed to go through a phenonium ion-like intermediate in which the electron enriched benzene ring is stabilized by its paramethoxyl group. The 4-methoxystyrene derivative is first observed upon creation of a double bond after an elimination reaction involving 1,8-diazabicyclo[5.4.0]undec-7-ene and the final product after a substitution reaction including a nucleophile of choice. The product is believed to be a result of the kinetic pathway of the reaction mechanism, and such a trend was observed during experimentation. This idea will be tested once an adequate amount of products are made and isolated, and research proceeds into optimization of the reaction. Some yields may be low due to inexperience at the start of the project, and the fact that optimization of the reactions has not taken place; it is important to remember that yields will likely increase. Future work will be focused on utilization of the 4-methoxystyrene derivative's unprotected olefin for polymerization, and/or formation of more complex molecules.

Principles of State Discovery in Decision Making

Mariah Ochoa, Mathematics Major

Mentor: Thomas Pouncy and Samuel Gershman, Ph.D.

Humans notice and adjust to changes in their environment, or state, without knowing the underlying causes of the change, and then decide whether to explore or exploit in order to obtain the most benefit. This remarkable ability to decipher when and how to use past information to generalize to novel situations is an unresolved problem in cognitive science. Human reinforcement learning models seek to provide a formal account of types of information humans use to make such decisions. This project focuses on capturing the participants' detection of state change and choice to explore/exploit regarding the state change. In an attempt to prompt this behavior, twenty-one participants were told to maximize their rewards within 200 trials using three buttons. For each trial, the buttons were within one of three unobservable reward distributions, or states, which were pulled stochastically such that each reward distribution was from either a previous state or a new state. We hypothesized that participants would detect state changes and that exploratory behavior would fluctuate systematically depending on the participant's belief regarding current hidden reward distributions. The experiment was found to need further adjustments to encourage participants to detect change rather than merely engage in exploration, which is being considered going forward.

Purification of the Cytoplasmic Domain of Serine/Threonine Phosphatase PstP and Phosphatase Assay with CwlM

Susana Pimentel, Biology and Microbiology Major

Mentor: Cara Boutte, Ph.D.

Mycobacterium tuberculosis (Mtb), the pathogenic agent of tuberculosis, undergoes cell wall changes to remain dormant in infected patients, in turn increasing phenotypic tolerance. The signaling mechanisms involving serine/threonine kinases (STPK) Mtb are not well understood. Mtb uses cell wall STPKs to regulate cell wall growth and division, and it is important to understand the mechanisms of these regulators in order to develop better treatments for tuberculosis. PknB is a STPK that phosphorylates CwlM, a protein that amplifies the activity of peptidoglycan precursor MurA. Under starvation stress, CwlM phosphorylation rapidly decreases, implying the presence of phosphatase activity. The central focus of this study was to discern if serine/threonine phosphatase PstP dephosphorylates CwlM. A vector that contained cytoplasmic domain of PstP (PstPc) was transformed into an expression strain of Escherichia coli and PstPc was successfully induced and purified. Purified aliquots of PstPc were made and then used to perform a phosphatase assay in vitro with phosphorylated CwlM. Proper analysis of the relationship between PstPc and CwlM could not be discerned due to PknB contamination, which kept CwlM phosphorylated. Adjusted experiments will be conducted in the future so that only purified phosphorylated CwlM and PstPc are involved in the phosphatase assay.

Calibration of Cantilever Beam Load Cell for Measuring Pressure and Shear in Prosthetic Socket Applications

Elida E. Sorto-Ramos, Aerospace Engineering Major

Mentor: Haiying Huang, Ph.D.

Advancing medical technology has enabled the complete and timely rehabilitation of a patient and the return to normal ambulation after amputation by use of prosthesis. The correct fit of the prosthesis is essential for comfort and increased quality of life. In order to better understand the forces at play at the delicate interface of the limb and the prosthetic socket, sensors must be developed. A cantilever beam load cell (CBLC) was developed to measure interfacial forces. With a pressure or shear force applied, the CBLC would deflect. This deflection was captured through strain gages that measure the change in resistance of a material due to elongation. The strain gages transmitted their signal to an Arduino microcontroller for data acquisition. The measured strains were used to inversely determine the pressure and shear that produced it. The measurement system was verified with theoretical calculations and computational analysis. Laboratory tests verified that the CBLC predicted the pressure induced on it within 1% of the actual value. The results produced a CBLC that can calibrate a patch antenna sensor for noninvasive measurement of interfacial stresses at the prosthetic socket-residual limb interface, as well as a variety of other biomedical applications.

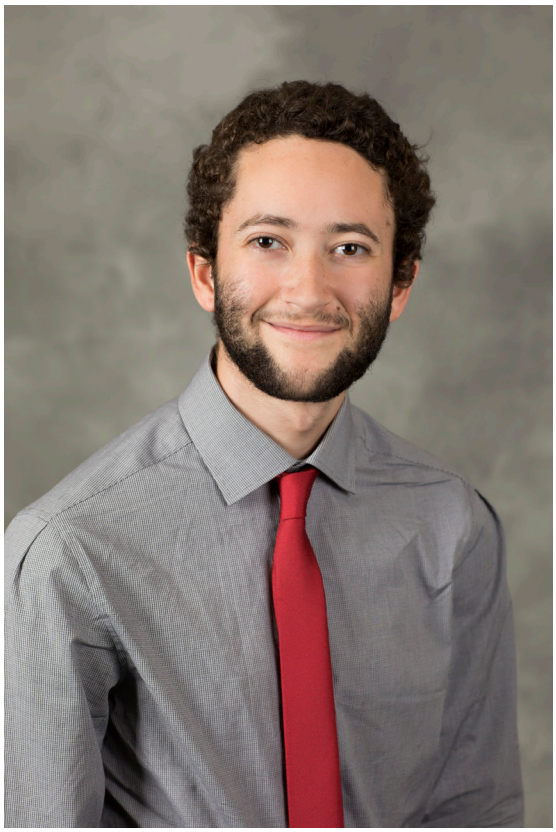

A Study on Possible Sizes of Matrix Factorizations

Andrew Soto-Levins, Mathematics Major

Mentor: David Jorgensen, Ph.D.

In 1980, David Eisenbud introduced a method of factoring polynomials using matrices: A matrix factorization of a polynomial p is a pair of n by n matrices A and B such that AB = pI_{n} and BA = pI_{n}. In this project, we explore several aspects of this idea. First we give the main theorem that says a polynomial written as the sum of n products has a matrix factorization of size 2^{n−1}. An easy corollary says that every polynomial in n variables has a matrix factorization of size 2^{n−1}. We then show that not every polynomial has a 2 by 2 matrix factorization over the real numbers. Another application of the main theorem shows that many different matrix factorizations of a given polynomial exist. In most cases, multiple different matrix factorizations of a particular size can be made and will look different. For this occurrence, we need a precise definition of equivalence: Let (A,B) and (A',B') be matrix factorizations of a polynomial p. These matrix factorizations are equivalent if there exists invertible n by n matrices alpha and beta such that beta A = A'alpha and alpha B = B'beta. We give examples of 2 by 2 matrices that are equivalent, and ones that are not.

ISSN 2642-2492